Lattice Element Models and Their Peculiarities

Mijo Nikolić, Emir Karavelić, Adnan Ibrahimbegovic, Predrag Miščević

▶ **To cite this version:**

Mijo Nikolić, Emir Karavelić, Adnan Ibrahimbegovic, Predrag Miščević. Lattice Element Models and Their Peculiarities. Archives of Computational Methods in Engineering, 2018, 25 (3), pp.753-784. 10.1007/s11831-017-9210-y . hal-01997368

HAL Id: hal-01997368
https://hal.utc.fr/hal-01997368

Submitted on 5 Feb 2019

HAL is a multi-disciplinary open access archive for the deposit and dissemination of scientific research documents, whether they are published or not. The documents may come from teaching and research institutions in France or abroad, or from public or private research centers.

L'archive ouverte pluridisciplinaire **HAL**, est destinée au dépôt et à la diffusion de documents scientifiques de niveau recherche, publiés ou non, émanant des établissements d'enseignement et de recherche français ou étrangers, des laboratoires publics ou privés.

Lattice Element Models and Their Peculiarities

Mijo Nikolić, Emir Karavelić, Adnan Ibrahimbegovic & Predrag Miščević

Archives of Computational Methods in Engineering
State of the Art Reviews

ISSN 1134-3060

Arch Computat Methods Eng
DOI 10.1007/s11831-017-9210-y

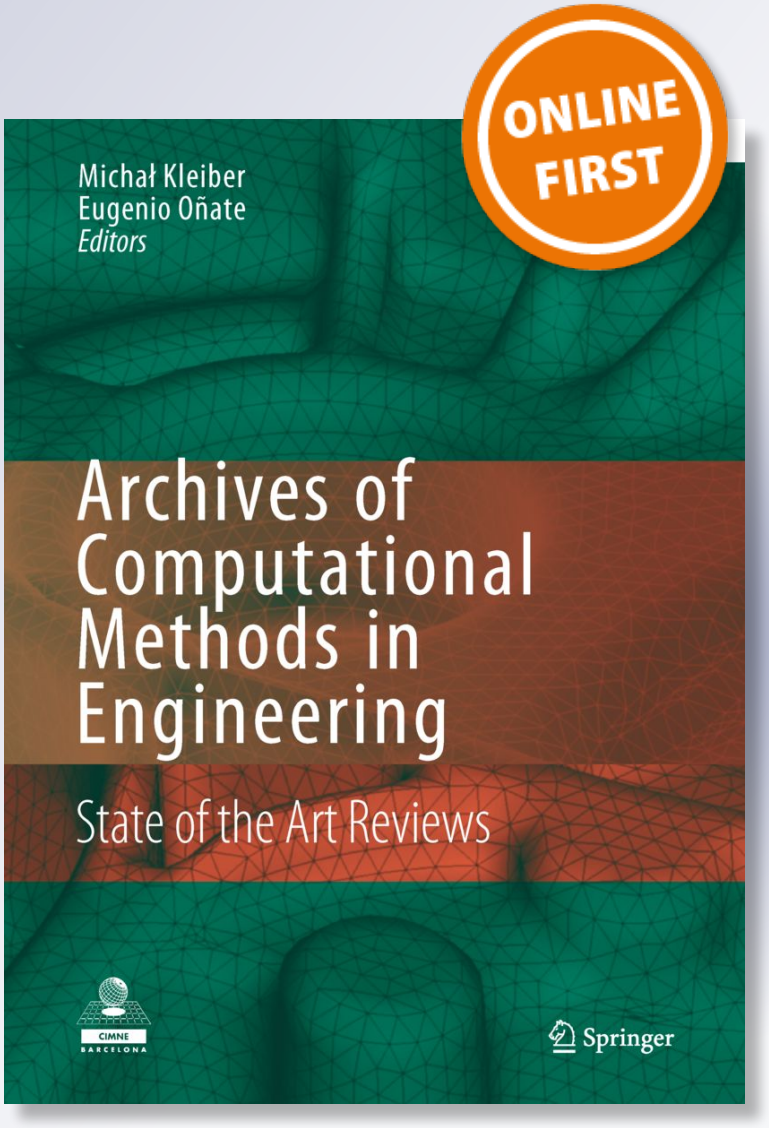

Springer

Your article is protected by copyright and all rights are held exclusively by CIMNE, Barcelona, Spain. This e-offprint is for personal use only and shall not be self-archived in electronic repositories. If you wish to self-archive your article, please use the accepted manuscript version for posting on your own website. You may further deposit the accepted manuscript version in any repository, provided it is only made publicly available 12 months after official publication or later and provided acknowledgement is given to the original source of publication and a link is inserted to the published article on Springer's website. The link must be accompanied by the following text: "The final publication is available at link.springer.com".

Author's personal copy

Arch Computat Methods Eng
DOI 10.1007/s11831-017-9210-y

ORIGINAL PAPER

Lattice Element Models and Their Peculiarities

Mijo Nikolić[1] · Emir Karavelić[2,3] · Adnan Ibrahimbegovic[4] · Predrag Miščević[1]

Received: 16 November 2016 / Accepted: 7 January 2017
© CIMNE, Barcelona, Spain 2017

Abstract This paper presents the lattice element models, as a class of discrete models, in which the structural solid is represented as an assembly of one-dimensional elements. This idea allows one to provide robust models for propagation of discontinuities, multiple cracks interaction or cracks coalescence. Many procedures for computation of lattice element parameters for representing linear elastic continuum have been developed, with the most often used ones discussed herein. Special attention is dedicated to presenting the ability of this kind of models to consider material disorder, heterogeneities and multi-phase materials, which makes lattice models attractive for meso- or micro-scale simulations of failure phenomena in quasi-brittle materials, such as concrete or rocks. Common difficulties encountered in material failure and a way of dealing with them in the lattice models framework are explained in detail. Namely, the size of the localized fracture process zone around the propagating crack plays a key role in failure mechanism, which is observed in various models of linear elastic fracture mechanics, multi-scale theories, homogenization techniques, finite element models, molecular dynamics. An efficient way of dealing with this kind of phenomena is by introducing the embedded strong discontinuity into lattice elements, resulting with mesh-independent computations of failure response. Moreover, mechanical lattice can be coupled with mass transfer problems, such as moisture, heat or chloride ions transfer which affect the material durability. Any close interaction with a fluid can lead to additional time dependent degradation. For illustration, the lattice approach to porous media coupling is given here as well. Thus, the lattice element models can serve for efficient simulations of material failure mechanisms, even when considering multi-physics coupling. The main peculiarities of such an approach have been presented and discussed in this work.

Keywords Lattice element model · Discrete element model · Material failure · Localized failure · Quasi-brittle failure · Embedded strong discontinuity · Mesh-independent softening · Multiple cracks

1 Introduction

Lattice element models, or simply lattice models, date back to the 1941 and the paper of Hrennikoff [1], in which he developed the grid-work method for modelling two-dimensional elastic continua with trussed framework system. This idea has been strongly evolving over the years resulting with many different lattice models presently. We could generally define the lattice models as an assembly of discrete one-dimensional elements for representation of structural solid. Such an evolution of this simple idea is not surprising taking into consideration the simplicity of the modelling of complex solids or structures with this approach and lighter computational cost. Moreover, efficient representation of some aspects, which are not easily tackled with

✉ Mijo Nikolić
mijo.nikolic@gradst.hr

[1] Faculty of Civil Engineering, Architecture and Geodesy, University of Split, Matice hrvatske 15, 21000 Split, Croatia

[2] Faculty of Civil Engineering, University of Sarajevo, 71000 Sarajevo, Bosnia and Herzegovina

[3] Lab. Roberval de Mecanique, Centre de Recherche Royallieu, UT Compiegne/ Sorbonne Universities, 60200 Compiègne, France

[4] Lab. Roberval de Mecanique, Centre de Recherche Royallieu, Chair for Computational Mechanics, UT Compiegne/ Sorbonne Universities, 60200 Compiègne, France

Published online: 03 February 2017

Author's personal copy

solid elements, like localized failure and cracking of the material make the lattice models very attractive.

Up to the present moment, many various lattice models have been developed for a number of applications. The main distinction between existing lattice models is how the lattice nodes interact between each other. This interaction of lattice nodes is defined through the behaviour of lattice elements which are shown in Fig. 1a in a simple triangular lattice. The choice of certain lattice model should be guided by the application requirements. Thus, one could choose a lattice with spring elements between the lattice nodes. In this version springs can be viewed as cohesive forces between the rigid particles of material, like shown in Fig. 1b. Depending on the application, the next choice would be whether normal, shear or rotational springs should be considered. The simplest model is when normal springs are used only to transfer the force between the particles. The most extensive model would be with the inclusion of all three mentioned springs in 2D. One could also make a choice with beams as lattice elements. Many beam lattices use Euler–Bernoulli theory, while Timoshenko beams provides more accurate response when elements in lattice are short and deep. Moreover, different values of Poisson's ratio are obtained with these two beam theories.

Variations with respect to lattice elements choice imply different corresponding procedures for obtaining lattice parameters. Namely, an important task with lattice computations is to use the correct stiffness of the lattice elements (springs or beams) in order to be able to simulate the corresponding equivalent continuum. It means that the lattice should be able to reproduce the linear elastic behaviour of the continuum solid and its uniform straining when uniform loading is applied. Lattice parameters are usually computed from this condition.

Simplicity and successful representation of localized failure and cracking mechanisms are the most important features that led to rapid development of lattice models. Namely, failure and cracking mechanisms can be simulated in a straightforward manner usually by detecting if any lattice element which represents the cohesive force between the particles has reached a certain failure criterion. If yes, cohesive fracture is initiated leading to gradual separation of the crack surfaces across the cohesive zone. The cohesive crack approach brings the benefit of avoiding the issue of singularity of the stress at the crack tip which is present in linear elastic fracture mechanics. Additionally, with lattice models, it is possible to simulate multiple cracks without worrying about multiple crack interactions. Various approaches are developed to deal with a post-peak behaviour of such elements. Classical approaches completely remove those failed elements and usually perform re-meshing of the lattice upon their removal. This leads to a very brittle response of the structure. Another approach is to model the post-peak behaviour of failed elements with progressive degradation of material stiffness leading to softening behaviour with fracture energy of material as input parameter. This results with gradual redistribution of internal forces to neighbouring elements and progressive failure. Softening behaviour of lattice elements is usually captured by sequentially linear algorithms trying to approximate the nonlinear softening curve. Classical damage or plasticity constitutive laws for softening can be used with nonlinear incremental iterative analysis.

If one would like to simulate cracking, the choice of lattice elements is very important to achieve this goal as well. Namely, for the prediction of correct crack path in shear tests, the shear and rotational degree of freedom should be used, either with shear and rotational springs or by using beam elements. It was shown in [2] that prediction of crack path in Nooru-Mohamed test with a lattice constructed from normal and shear springs failed, with crack propagating straight. When the rotational spring was introduced, the crack could curve, and a pattern similar to the one in the experiment was obtained. Another important choice for prediction of correct crack pattern is lattice regularity. We can distinguish here between regular (periodic lattice with structured grid) and irregular lattices with disordered topology (unstructured grid). It is much easier to achieve the uniform straining with a regular lattice. However, it can also strongly bias the cracking patterns with its structured grid. On the contrary, irregular lattices provide lower predetermination of cracking direction but generally do not provide uniform straining. It is important to emphasize that the procedure for the computation of lattice parameters significantly differs in these two cases. The procedures for obtaining lattice parameters in various models with springs and beams can be found in the extensive overview of lattice models by Ostoja-Starzewski [3].

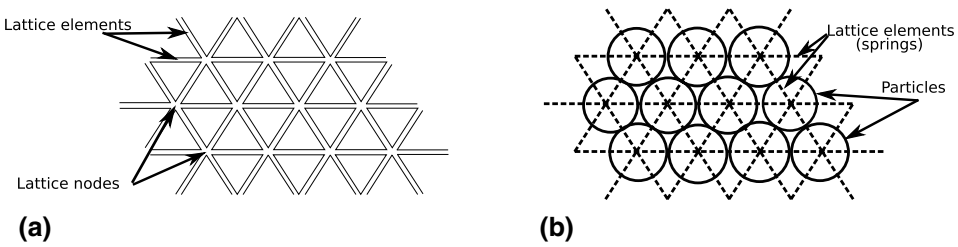

Fig. 1 **a** Lattice network with marked lattice nodes and elements **b** lattice network with springs

Author's personal copy

It is well known that disorder can strongly influence the failure mechanisms. Lattice models possess a natural ability of considering disorder through material heterogeneities and representation of different multi-phase materials with interactions between their phases. Another important aspect which can strongly influence the failure mechanism is the size of the localized zone, i.e. fracture process zone, which forms around the propagating crack. Narrow localized zone produces less dissipated energy resulting with brittle failure. Wider localization is associated with more ductile behaviour. The size of the localized fracture process zone stands as an universal issue in various models trying to simulate cracks and discontinuities. In linear elastic fracture mechanics, the amount of plastic dissipation related to the size of the localized fracture process zone around the crack tip is important for not underestimating material properties. Standard finite elements dealing with failure in softening produce non objective and mesh dependent results, which is also related to the size of the localized zone where finer mesh produces narrower zone of localization and consequently more brittle response. In order to fully understand the size of the localized zone, one could use molecular dynamics framework in which interactions between the atoms and molecules are observed taking into consideration disorder at the atomistic scale. However, this approach requires complicated inter-atomic potentials and a significant computational power. On the contrary, lattice models are less computationally demanding and can capture disorder, as well as stabilized localization zone. These favourable properties lead to the vast usage of lattice models in simulating the behaviour at finer scales of the material, like micro-scale and meso-scale, where the material can be observed as collection of particles in equilibrium with their interaction forces. Application to many materials ranging from metals, composites, ceramics and polymers to granular materials can be found in the literature. However, the development and evolution of lattice models were mostly influenced by the industrial requirements for the composite materials, especially concrete. It is well known that physical properties of concrete strongly depend on the composition of material at lower scales. Many authors were trying to simulate concrete at meso-scale, which can be observed as a two or three phase composite with aggregates surrounded by cement paste and interface transition zone. One approach at concrete meso-scale, like shown in [4, 5], is by overlapping digital images of concrete internal structure onto the lattice and assigning different material properties to the lattice elements, whether the lattice element coincide with aggregate, cement paste or interface. Meso-scale models can capture fundamental aspects of heterogeneity. Micro-scale refers to the size of several micrometers and hardened cement paste with capillary pores filled with liquid water and vapour. Concrete micro-scale can be captured not directly by overlapping lattice, but by introducing variations in material by statistical distributions. Lattice models can also be used at macro-scale, that is the usual engineering scale, for simulations of fracture propagation. This is usually performed under quasi-static conditions, but dynamic environment can be simulated as well.

Recently, a number of powerful lattice models has been published. One of the most recent novel features is the introduction of embedded strong discontinuity into lattice truss bar elements [6, 7], and beam elements [8, 9]. The embedded strong discontinuity comes as a result of introducing the Dirac delta function into the lattice elements to represent the displacement jumps between the particles, corresponding to crack openings. The formulation based on embedded strong discontinuity acts as a localization limiter and stabilizes the localized zone, producing the release of fracture energy independently of the chosen mesh. Another recent feature is the application of the contact between the particles, typical for classical discrete element models. The latter is important for fragmentation under compression test. Contact detection and interaction between the released particles are enabled after the removal of the broken cohesive links [10, 11]. The contact can also be modelled between the load platens and the specimen constructed from lattice elements [12, 13]. Moreover, lattice models have been recently used in solving the transport problems in cracked heterogeneous materials. Among them, interaction between the mechanical aspects captured by lattice models and fluid flow can be found in [14–17]. The future potential lies in the further development of lattices for solving fluid problems, hydraulic fracturing problems or applications in partially-saturated soils. Moreover, the potential could be in other multi-physics applications as well.

The intention of this paper is to give the reader an extensive overview of lattice models and their peculiarities. Complex phenomena related to failure of the materials can be simulated with lattice models, yet they are still simple and computationally not very demanding. This paper also provides very recent developments and advances in the field of lattice element modelling.

The outline of this paper is as follows. In Sect. 2 we give a brief overview of various existing lattice approaches. We also discuss the procedures for obtaining lattice parameters and provide parameters for most used lattices. Section 3 is dedicated to applications of lattice models on material failure and cracking mechanisms. Issues related to numerical instabilities occurring in failure and softening are also addressed here. In Sect. 4, we discuss the implementation of embedded strong discontinuities into the framework of lattice models. Section 5 pertains to the influence of

Author's personal copy

transport in material failure and multi-physics application of fluid-structure interaction with lattice models, which can be used to represent the cracking under the influence of fluid flow. Conclusions are given at the end of the paper.

2 Topology of Lattice Element Models

This section provides an overview of various lattice models, with respect to lattice topology. Lattice-spring and lattice-beam models are addressed here as well. The main distinction with respect to topology is the grid regularity. Two major groups can be extracted: regular lattices with structured grid and irregular lattices with disordered and unstructured grid. The stress-strain relationship of the material should be derived based not only on the material properties, but also on the geometric properties of the underlying lattice structure to obtain uniform straining of the lattice. Regular or irregular lattice topologies imply different computation of lattice element parameters. Regular lattices can easily represent uniform straining when the material is uniformly loaded, while the irregular ones are better for representation of crack patterns in heterogeneous materials.

2.1 Regular Lattices

A regular lattice, or a lattice with structured grid, may be squared or triangular (Fig. 2). It is periodic, where the unit cell can be considered as a repeating element in the mesh (Fig. 2). The lattice can also be periodic, but with disordered topology, where the inner structure of the unit cell is not necessarily nicely ordered, but it repeats itself in space. We will first introduce the lattice-spring models which use springs to transfer forces between the particles. These springs can be normal, shear or rotational ones (Fig. 3). Then, we will introduce lattice-beam models as a natural extension of the lattice-spring models.

2.1.1 Lattice-Spring Models

The basic idea in setting up the lattice-spring models is based on the equivalence between the strain energy stored

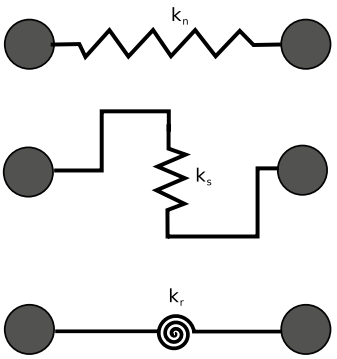

Fig. 3 Spring as a cohesive link between the two nodes. Three types of springs: normal spring k_n, shear spring k_s and rotational spring k_r

in a unit cell of lattice structure (which represents the repeating element in the mesh and is connected by springs to its neighbours) and the continuum strain energy

$$E_{cell} = E_{continuum} \tag{1}$$

A periodic unit cell in triangular and squared lattice is shown in Fig. 2. The strain energy of a lattice-spring model can be computed as the sum of energies of single bonds

$$E_{cell} = \frac{1}{2}\sum_{b}^{N_b}(F \cdot u)^{(b)} \tag{2}$$

where b denotes the b-th spring, F is a force on the spring b and u is the displacement of the spring b. Corresponding continuum strain energy can be expressed as a volume integral in the continuum model

$$E_{continuum} = \frac{1}{2}\int_{V} \sigma \cdot \epsilon dV \tag{3}$$

where σ and ϵ are the stress and strain, respectively. If one wants to obtain uniform strain fields with a lattice, these two energies can be used to relate the stiffness tensor containing spring constants and the one containing continuum constants. Lattice parameters can be derived from this relation. While the procedure for deriving the parameters for various lattices can be found in [3], the frequent example of triangular lattice with springs is presented here. Triangular lattices have hexagonal unit cells like shown in Fig. 4. Unit

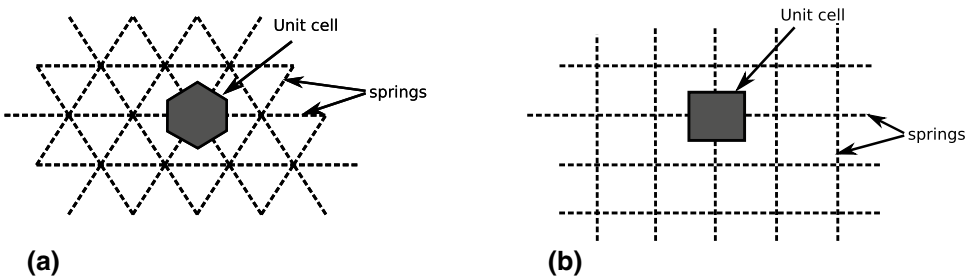

Fig. 2 **a** Regular triangular lattice network with springs **b** regular square lattice network with springs

Author's personal copy

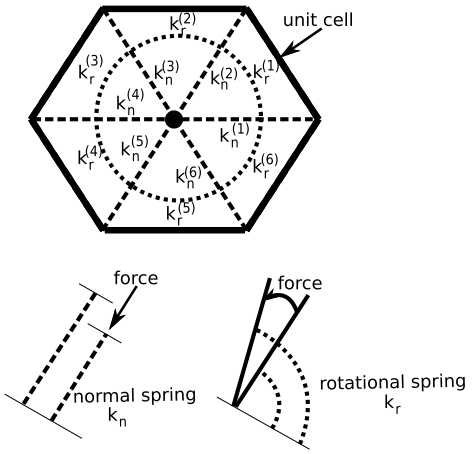

Fig. 4 Unit cell in triangular lattice with normal and rotational springs

cells can be connected to their neighbours by normal, shear or rotational springs, and their combinations.

If the normal springs in triangular lattice are used only, we obtain the so called triangular lattice with central interactions where normal force on the spring can be expressed as

$$F_i = k_n^{(b)} n_i^{(b)} n_j^{(b)} u_j \;\; ; \;\; i,j = 1,2 \tag{4}$$

where k_n is the normal spring constant, while n represents spring unit vectors. This model can be used to represent in-plane elasticity in two dimensions where the corresponding constitutive law is given by

$$\sigma_{ij} = C_{ijkm} \epsilon_{km} \;\; ; \;\; i,j,k,m = 1,2 \tag{5}$$

and C_{ijkm} is the stiffness tensor of continuum constants. If the springs are of length l and positioned at the angles of 0∘, 60∘ and 120∘ in the mesh, the area of the unit cell is $V = 2\sqrt{3}l^2$ and the stiffness tensor can be related to the spring network by

$$C_{ijkm} = \frac{1}{2\sqrt{3}} \sum_{b=1}^{6} k_n^{(b)} n_i^{(b)} n_j^{(b)} n_k^{(b)} n_m^{(b)} \tag{6}$$

Taking all spring constants $k_n^{(b)}$ to be the same k_n results with

$$\begin{aligned} C_{1111} &= C_{2222} = \frac{9}{8\sqrt{3}} k_n \\ C_{1122} &= C_{2211} = C_{1212} = \frac{3}{8\sqrt{3}} k_n \end{aligned} \tag{7}$$

With such computed lattice parameters, where only one independent elastic constant k_n exists, one can use the regular triangular lattice-spring model with only normal springs to model the isotropic continuum. Here, classical Lamé constants are obtained from (7)

$$\lambda = \mu = \frac{3}{8\sqrt{3}} k_n \tag{8}$$

The planar anisotropy considers six independent material constants C_{ijkm}. In order to successfully model the anisotropic case with six independent parameters, three different normal spring constants $k_n^{(b)}$ should be used, together with rotational springs $k_r^{(b)}$. Moreover, rotational springs are used for Poisson's ratio variation. The unit cell for this model contains six normal springs and six rotational springs (Fig. 4). While the normal springs are represented by a spring constant k_n, rotational springs have a spring constant k_r which provides the relation between the change in the angle between two neighbouring normal springs and the corresponding force. Since the unit cell is symmetric, twelve constants reduce to six independent ones (3 axial and 3 rotational springs). The angle change between two adjacent springs (b) and $(b+1)$ is measured by $\Delta\Phi = \theta^{(b+1)} - \theta^{(b)}$ and the energy stored in the rotational spring is

$$E^{(b)} = \frac{1}{2} k_r^{(b)} |\Delta\Phi|^2 \tag{9}$$

Summing the energies over the cell of all normal and rotational springs and comparing it to the stiffness tensor leads to the derivation of the elastic moduli for this anisotropic spring model. With this model we can also represent isotropic material if we assume that all normal springs have the same value k_n and all rotational spring constants have the same value k_r. This is known as the Kirkwood model [18]. In this case, two independent constants exists which are related to the continuum constants by the following equations (see also [3])

$$\begin{aligned} C_{1111} &= C_{2222} = \frac{1}{2\sqrt{3}} \left(\frac{9}{4} k_n + \frac{1}{l^2} k_r \right) \\ C_{1122} &= C_{2211} = \frac{1}{2\sqrt{3}} \left(\frac{3}{4} k_n - \frac{9}{4l^2} k_r \right) \\ C_{1212} &= \frac{1}{2\sqrt{3}} \left(\frac{3}{4} k_n + \frac{9}{4l^2} k_r \right) \end{aligned} \tag{10}$$

Two material constants, planar bulk modulus (κ) and shear modulus (μ) can be derived from relations (10)

$$\begin{aligned} \kappa &= \frac{1}{2\sqrt{3}} \left(\frac{3}{2} k_n \right) \\ \mu &= \frac{1}{2\sqrt{3}} \left(\frac{3}{4} k_n + \frac{9}{4l^2} k_r \right) \end{aligned} \tag{11}$$

while Poisson's ratio (ν) can vary between 1/3 and -1

Author's personal copy

$$\nu = \frac{1 - \frac{3k}{k_n l^2}}{3 + \frac{3k_r}{k_n l^2}} \tag{12}$$

One can use a slightly different, Keating model [19], with a different calculation of the energy stored in rotational springs resulting with a different range of Poisson's ratio: from $-1/3$ to $1/3$.

Among these, Born model [20] can be considered as well. It is a model in which axial and shear forces can be transferred between the particles via normal and shear springs. However, this model is not rotationally invariant. Another model in which axial and shear force are transmitted between the particles neglecting their rotations is the confinement shear lattice model [21].

Since the introduction of rotational degrees of freedom into the lattice spring models provides the stiffness matrix resembling the beam stiffness matrix, beams come as a natural choice to represent lattice elements.

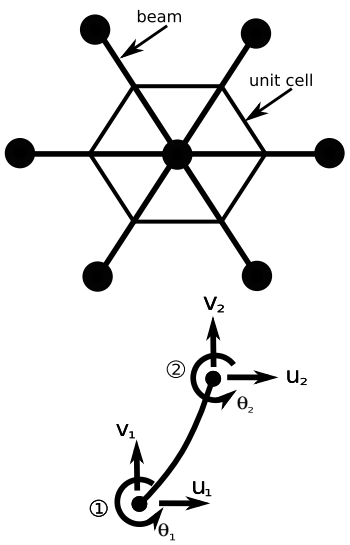

Fig. 5 Unit cell connected to neighbours by beams. Beam node can carry two translational degrees of freedom and one rotational

2.1.2 Lattice-Beam Models

In the lattice-beam models, lattice nodes which can be considered as the centres of the unit cells, are connected by beams that can carry normal force, shear force and bending moment. Thus, each lattice node contains three degrees of freedom (in 2D), two translational u_i, v_i and one rotational θ_i (Fig. 5). When the lattice elements are chosen as beams, the lattice network becomes a frame structure. Beam lattices are used to represent the so-called micro-polar continuum. We can choose the classical Euler–Bernoulli and Timoshenko beams as lattice elements, while the latter should be used when beam elements in the lattice are short and deep.

The relationships between the properties of a continuum phase and its representative beams in the lattice is again obtained by comparing the strain energies accumulated in continuum and lattice unit cells, according to Eq. (1). The shape and size of the unit cell depend on the mesh configuration, while the frequently used ones are again triangular and squared beam lattices (Fig. 6). The strain energy of the beams in the hexagonal cell can be written as

$$E_{cell} = \frac{1}{2}\sum_{b=1}^{6}\left(F^{(b)}\gamma^{(b)} + Q^{(b)}\tilde{\gamma}^{(b)} + M^{(b)}\kappa^{(b)}\right)\frac{l^{(b)}}{2} \tag{13}$$

where $F^{(b)}$, $Q^{(b)}$ and $M^{(b)}$ are the normal force, shear force and moment of each beam. That can be obtained from the constitutive equations of Euler–Bernoulli beam

$$\begin{aligned} F^{(b)} &= E^{(b)}A^{(b)}\gamma^{(b)} \\ Q^{(b)} &= \frac{12E^{(b)}I^{(b)}}{(l^{(b)})^2}\tilde{\gamma}^{(b)} \\ M^{(b)} &= E^{(b)}I^{(b)}\kappa^{(b)} \end{aligned} \tag{14}$$

where γ is axial strain, $\tilde{\gamma}$ is the difference between the rotation angle of the beam and the rotation angle of its end node and κ is the curvature. The full derivation of lattice beam parameters can be found in [3]. Additional derivation of regular triangular beam lattice models can be found in [22], where the authors use triangular Euler–Bernoulli beam lattice and equivalent lattice spring model with three springs, normal, shear and rotational. They have shown that

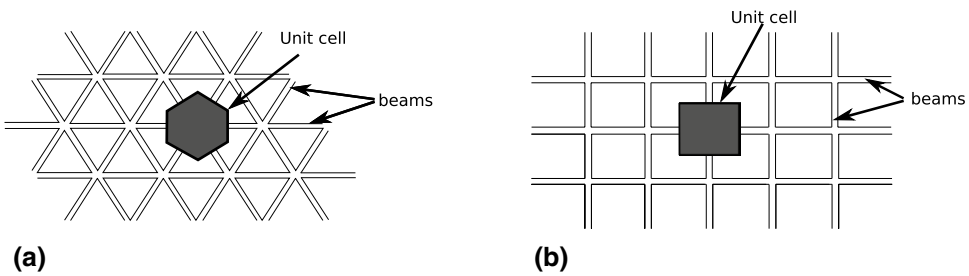

Fig. 6 Lattice-beam models **a** regular triangular lattice **b** regular square lattice

Author's personal copy

Table 1 Continuum properties related to lattice spring and lattice beam properties

Continuum	Lattice spring	Lattice beam
ν	$\frac{k_n-k_s}{3k_n+k_s}$	$\frac{1-\left(\frac{h}{l}\right)^2}{3+\left(\frac{h}{l}\right)^2}$
G	$\frac{\sqrt{3}}{4}(k_n+k_s)$	$\frac{\sqrt{3}}{4}\left(\frac{E^{(b)}A^{(b)}}{l}+\frac{12E^{(b)}I^{(b)}}{l^3}\right)$
E	$\frac{2\sqrt{3}k_n(k_n+k_s)}{3k_n+k_s}$	$2\sqrt{3}\frac{1+\left(\frac{h}{l}\right)^2}{3+\left(\frac{h}{l}\right)^2}\frac{E^{(b)}A^{(b)}}{l}$

Table 2 Lattice spring related to continuum and lattice beam properties

Lattice spring	Continuum	Lattice beam
k_n	$\frac{E}{\sqrt{3}(1-\nu)}$	$\frac{E^{(b)}A^{(b)}}{l}$
k_s	$\frac{2G(1-3\nu)}{\sqrt{3}(1-\nu)}$	$\frac{12E^{(b)}I^{(b)}}{l^3}$
k_r	$\frac{1}{\sqrt{3}}\left(\kappa-\frac{G(1-3\nu)}{6(1-\nu)}l^2\right)$	$\frac{E^{(b)}I^{(b)}}{l}$

these two lattices are equivalent and can identically represent micro-polar continuum if the spring constants are expressed through the following beam properties

$$k_n = \frac{E^{(b)}A^{(b)}}{l}$$
$$k_s = \frac{12E^{(b)}I}{l^3} \tag{15}$$
$$k_r = \frac{12E^{(b)}I}{l}$$

Moreover, Euler–Bernoulli beam lattice and equivalent spring lattice are related to the underlying continuum. Linking the stress strain relationships of the lattice beam, lattice spring and continuum model leads to the connection between the continuum variables and the spring constants in a lattice spring system or to the beam properties in a lattice beam system. The full procedure is explained in [22], while the final expressions and the connection between these models are presented in Tables 1, 2, and 3.

When the beams used in the lattice are short and deep, resulting with stubby connections (Fig. 7), it is more appropriate to use Timoshenko beam elements. The unit cell strain energy is again obtained from Eq. (13), the same as for Euler–Bernoulli beam, except that the shear force is computed differently and comes from Timoshenko beam governing equations

$$Q^{(b)} = \frac{12E^{(b)}I^{(b)}}{(l^{(b)})^3(1+\beta)}l^{(b)}\tilde{\gamma}^{(b)} \tag{16}$$

Table 3 Lattice beam properties related to continuum and lattice spring properties

Lattice beam	Continuum	Lattice spring
$\frac{h}{l}$	$\sqrt{\frac{1-3\nu}{1+\nu}}$	$\sqrt{\frac{k_s}{k_n}}$
$E^{(b)}$	$\frac{E}{\sqrt{3}(1-\nu)\sqrt{\frac{1-3\nu}{1+\nu}}}$	$k_n\sqrt{\frac{k_n}{k_s}}$

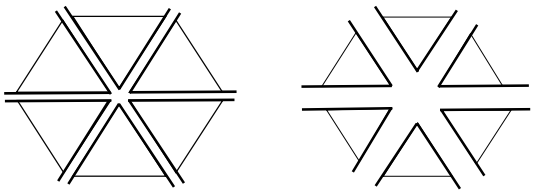

Fig. 7 Slender (Euler–Bernoulli) and stubby (Timoshenko) beams in a unit cell

where β is the dimensionless ratio of bending to shear stiffness

$$\beta = \frac{12E^{(b)}I^{(b)}}{G^{(b)}A^{(b)}l^2} \tag{17}$$

The paper [23] presents the Timoshenko beam lattice, with its extensive derivations, for the fracture of a composite structure. The basic relations between continuum constants, modulus of elasticity and Poisson's ratio, and Timoshenko beam lattice are given in Table 4.

2.2 Irregular Lattices

In the previous subsection, we described the lattice-spring and lattice-beam models with regular geometries. It has been noted that regular lattices can represent elastically uniform behaviour due to the symmetry of the mesh and periodicity of the unit cell in which strain energies are computed to derive the lattice parameters. However, regular geometry in a lattice can influence the biased crack propagations. Irregular lattices or random geometry lattices can greatly reduce this effect, but are not generally elastically uniform under uniform straining.

It has been shown in [24] that scaling of element stiffness terms in irregular lattice based on a Voronoi discretization of the domain results in homogeneous response of the material under uniform straining. This can be valid for both, lattice-spring and lattice-beam models.

Voronoi tessellation can be constructed from a random set of points distributed all over the domain, by assigning to each point the part of the domain which is closer to it than to any other of the chosen points. This point represents the nucleus

Author's personal copy

Table 4 Continuum properties related to the Timoshenko beam lattice properties

Continuum	Lattice beam
ν	$\frac{1-\left(\frac{h}{l}\right)^2 \frac{1}{1+\beta}}{3+\left(\frac{h}{l}\right)^2 \frac{1}{1+\beta}}$
E	$2\sqrt{3}E^{(b)}\frac{h}{l}\frac{1+\left(\frac{h}{l}\right)^2 \frac{1}{1+\beta}}{3+\left(\frac{h}{l}\right)^2 \frac{1}{1+\beta}}$

of the Voronoi cell. The domain is then covered by non overlapping polygons Ω_i corresponding to point P_i with a rule

$$\Omega_i = \left(P \;\; such \;\; that \;\; d(P,P_i) \leq d(P,P_j), \;\; \forall j \neq i\right) \tag{18}$$

where $d(.,.)$ denotes the distance in the Euclidean space. It follows that each side of a Voronoi cell splits the distance $d(P_i,P_j) = l_{ij}$ in half (see Fig. 8). This is an important property by which the scaling of the lattice properties will be performed.

According to the random distribution process, the nuclei can be more or less uniformly distributed. The details of the Voronoi tessellation can be found in [25]. It is worth noting that the Voronoi tessellation is dual to the Delaunay triangulation, and either discretization can be derived from its corresponding dual (Fig. 9). This is a very convenient property in lattice networks, where Delaunay edges can be regarded as lattice elements and their geometrical properties can be extracted from Voronoi cells.

Bolander et al. [24, 26, 27] developed irregular spring lattices for quasi-static crack propagation. They have shown that the stiffness of the spring lattice with normal k_n, shear k_s and rotational k_r springs can be scaled according to the Voronoi diagram (Fig. 8) as

$$\begin{aligned} k_n &= \frac{EA_{ij}}{l_{ij}} \\ k_s &= \frac{EA_{ij}}{l_{ij}} \\ k_r &= \frac{k_n h_{ij}^2}{12} \end{aligned} \tag{19}$$

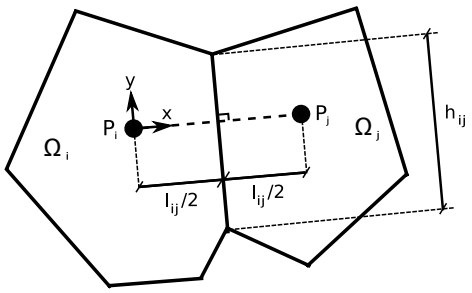

Fig. 8 Two neighbouring 2D Voronoi cells

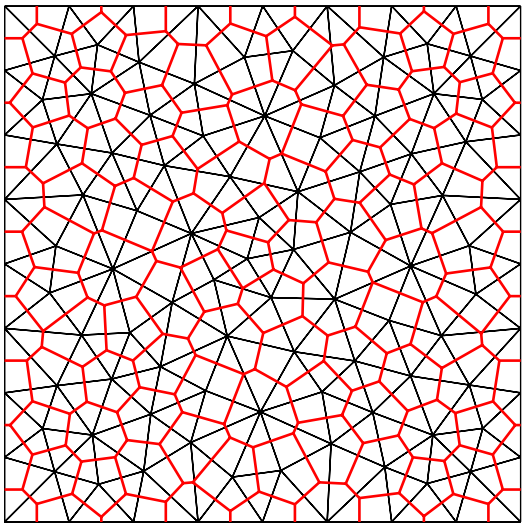

Fig. 9 2D irregular lattice with Voronoi tesselation. Delaunay triangulation and Voronoi tesselation are corresponding duals. (Color figure online)

This stiffness is dependent on the distance l_{ij} between the lattice nodes i and j, and the length of the neighbouring Voronoi edge h_{ij}. The $A_{ij} = h_{ij} \cdot t$ can represent the cross section area of the lattice element, where t is thickness when 2D case is considered. Such scaling of spring stiffness parameters results with an elastically homogeneous continuum representation. However, if $k_n \neq k_s$, the lattice is not going to be homogeneous.

Scaling of the stiffness presented in relations (19), can also be used in a 3D case (see also [27])

$$\begin{aligned} k_n &= k_{s1} = k_{s2} = \frac{EA_{ij}}{l_{ij}} \\ k_{\phi a} &= \frac{EJ_p}{l_{ij}}; \;\; k_{\phi s1} = \frac{EI_{11}}{l_{ij}}; \;\; k_{\phi s2} = \frac{EI_{22}}{l_{ij}} \end{aligned} \tag{20}$$

where A_{ij} is now the Voronoi facet area representing the common area of the two neighbouring 3D Voronoi cells (Fig. 10), J_p is the polar moment of inertia, I_{11} and I_{22} are the two principal moments of inertia of the facet area (Fig. 11).

It is generally more difficult to obtain the uniformity of the beam lattice with irregular mesh. One way is to use a special case of square beam lattice with Voronoi scaling where axial beam components are dominant [24]. An alternative way to compute lattice parameters to obtain homogeneous lattice response presented in [2] is based on an iterative process of searching for the right combinations of the parameters. Although, irregular beam lattices with parameters computed from Voronoi scaling do not necessarily provide elastic uniformity of all nodes and lattice elements, it has been shown that their macroscopic responses correspond to the equivalent continuum responses and no

Author's personal copy

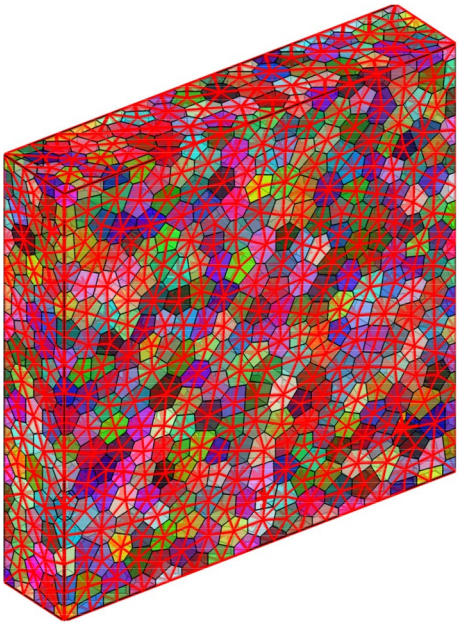

Fig. 10 3D irregular lattice with Voronoi cells. (Color figure online)

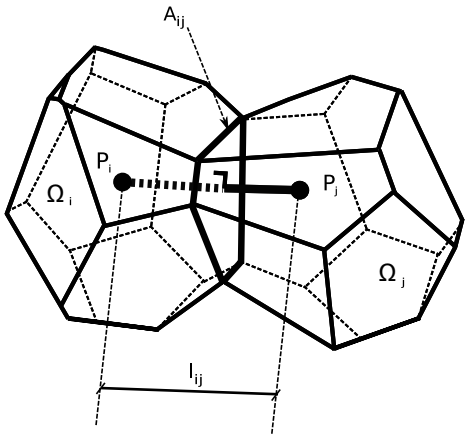

Fig. 11 Two neighbouring 3D Voronoi cells

global stiffness is gained or lost with this way of computing parameters [8]. The amount of straining disorder introduced into the beam lattice with irregular mesh depends on the disorder of the mesh. Many present lattice-beam models use Voronoi scaling or similar variations to compute the lattice parameters in the case of irregular meshes. Euler–Bernoulli beams with Voronoi scaling are used to construct lattice elements in [10, 11]. The same scaling procedure is used with Timoshenko beams in [8, 9]. In [12, 13, 21], a similar procedure with a modification such that the vertices of the Voronoi cells correspond to the centres of the masses of the underlying Delaunay triangles is used. In [28–30], a lattice element similar to Euler–Bernoulli beam is developed according to the Voronoi scaling. All these works are dealing with meso-scale of heterogeneous materials like concrete or rocks where straining is not uniform. The main concern of the models is to successfully represent cracking patterns with respect to material heterogeneities, while very often an additional disorder through statistical distributions due to variations in material properties is also needed.

3 Failure Modelling with Lattice Element Models

3.1 Failure of the Materials

One of the important goals scientists and engineers have been tackling for a long period of time is how to describe the failure and fracturing of materials. When the material is homogeneous and the crack is predetermined, one could predict the failure mechanism. However, most materials are heterogeneous and their failure mechanisms become very complex due to the influence of heterogeneities, occurrence of multiple cracks merging together or plastic deformations.

An essential part of dealing with failure is to define the criterion which states when the fracture will propagate. One of the classical approaches is based on the energy balance proposed by Griffith [31]. It considers a crack of area A (crack length in two dimensional problems) propagating due to external forces by an amount of dA. Griffith defined the energy release rate as

$$G = \frac{dW - d\epsilon}{dA} \tag{21}$$

where dW is an increment of the work of externally applied loads and $d\epsilon$ is an increase of elastic potential energy of the system available for the crack growth. The creation of the crack will use some additional energy equal to $2\gamma_s dA$, with γ_s as a crack surface energy. This criterion states that the crack will propagate if the release of the energy from the system is larger than the energy required for the crack to propagate:

$$G \geq G_c. \tag{22}$$

The critical energy release rate $G_c = 2\gamma_s$ represents the internal characteristics of the material. The Griffith criterion is very applicable in linear elastic fracture mechanics, but it lacks the possibility to consider additional dissipation of the energy G due to plastic deformation and micro cracks.

Another criterion is to use the stress intensity factors K developed by Irwin [32], which participate in the equation for stress at the vicinity of the crack tip

$$\sigma_{ij}^{(k)}(r,\theta) \approx \left(\frac{K_{(k)}}{\sqrt{2r\pi}}\right) f_{ij}^{(k)}(\theta) \tag{23}$$

Author's personal copy

where σ_{ij} are the Cauchy stresses, r is the distance from the crack tip, θ is the angle with respect to the plane of the crack, and $f_{ij}(\theta)$ is a dimensionless function depending on the angle θ and the fracture mode (k) (fracture modes are shown in Fig. 12). The critical stress intensity factors K_{Ic}, K_{IIc}, K_{IIIc} for all failure modes can be obtained.

It can be shown that the works of Irwin and Griffith can be made equivalent and that Eq. (23) is valid in linear elastic fracture mechanics. One can notice that when the distance to the crack tip r tends to zero, Cauchy stress goes to infinity. However, stress at the crack tip is not singular in reality, because a small localized zone in which nonlinear and dissipative processes occur (called fracture process zone) is created in a neighbourhood very close to the propagating crack tip. Thus, Eq. (23) is valid outside of this fracture process zone, where material behaviour is linear elastic. This disadvantage of the mentioned approach was manifested in the underestimation of the critical failure strength of many ductile materials. Irwin proposed a modification [32] based on Orowan's findings [33], in which he included an additional energy term due to plastic work near the crack tip

$$G_c = 2\gamma_s + \gamma_p \tag{24}$$

where γ_p is the term due to plastic dissipation. The same approach is applied for damaged materials in which a small zone of microcracks is created instead of plastic deformation.

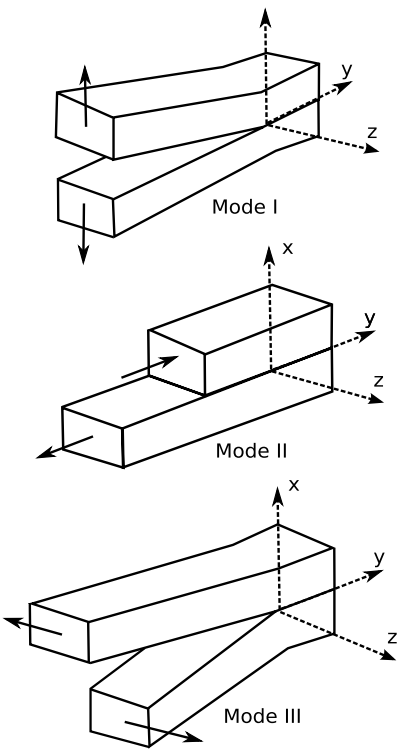

Fig. 12 Three failure modes: Mode I is the opening mode, Mode II is the in plane shearing mode, and Mode III is the out of plane tearing mode

In most real materials which exhibit nonlinear and inelastic behaviour, the localized plastic zone near the crack tip is not necessarily in a region closest to the crack, but it may be spread wider and even change during the crack growth. Linear elastic fracture mechanics is not applicable in these cases. Moreover, heterogeneities can induce distortions of the crack front and modify the values of stress intensity factors. Therefore, more general theories are needed for such materials. Among them, an important criterion for fracture propagation which can consider nonlinear elastoplastic materials is the J-integral developed by Rice [34], which calculates a contour integral around the crack tip

$$J = \int_{\Gamma} \left(wn - T_i \frac{\partial u_i}{dx} \right) d\Gamma \tag{25}$$

where w is the strain energy density, T_i are the components of traction, u_i are displacement components, and n is a unit vector normal to the crack contour Γ. In a case of linear elastic material, the J-integral can be reduced to Griffith theory and made equivalent to the energy release rate G.

As indicated in [35], the localized plastic zone or localized damage zone around the propagating crack can be considered as a small scale cut-off distance of the elastic solution. It is crucial to correctly identify this distance since it has a significant effect on the response of the cracked material and influences energy dissipation. Thus, one can measure the stress or the stress intensity factor outside of the cut-off distance by the Eq. (23) which holds true for linear elasticity.

Previous approaches can be applied in linear elastic fracture mechanics to ideal homogeneous materials or to real materials with fracture process zone, when the failure is ruled by a single crack. On the contrary, failure of a vast number of real materials (especially brittle ones) is strongly governed by disorder, mainly pertaining to heterogeneities, which complicate the failure mechanisms even more. Namely, the occurrence of multiple cracks which can coalesce, branch or simultaneously grow, while singular stresses at the crack tips interact with each other, require more detailed description and understanding of the heterogeneous nature of the material. Additional criteria for fracture propagation are needed to create new interfaces, together with corresponding contributions from plasticity and damage at the crack tips. According to [35], the response of the structure with multiple cracks is not unique when Griffith criterion or criterion based on stress intensity factor is used.

Many experiments have shown that heterogeneities rule the phenomenon of fracture. For example, two pieces of the same material will not produce identical crack paths

Author's personal copy

nor macroscopic responses. The latter usually exhibits the decreasing curve, called strain softening, representing a material instability which occurs under the failure. Such instability is characterized by the decreasing stresses even with increasing strains. It has been shown that the softening curve depends on the size of the localized zone in which damage or plasticity are concentrated. This phenomenon can also be confirmed with standard finite elements, in which softening and the localized zone are mesh dependent. Namely, the damage becomes more localized when refining the finite element mesh, leading to mesh dependent mechanical response (Fig. 13). In order to provide mesh-independent softening response, localization needs to be stabilized. Several methods called localization limiters (see [36]) have been proposed to deal with localization producing the mesh-independent results. Some of them use the mesh-dependent value of softening modulus to provide the desired dissipation and do not require any modification of the theoretical formulation. The same can be achieved by localization limiter based on viscoplastic regularization. Another class of localization limiters is based on non-local theory of plasticity [37] or non-local damage formulation [38]. In non-local theory, stresses are computed from the average of strains in the chosen neighbourhood defined by the characteristic length, which can span several finite elements. However, an important disadvantage of the non-local theory is the lack of the physical basis for choosing the appropriate value of the characteristic length. The reader is referred to reference [36] for more details on localization limiters.

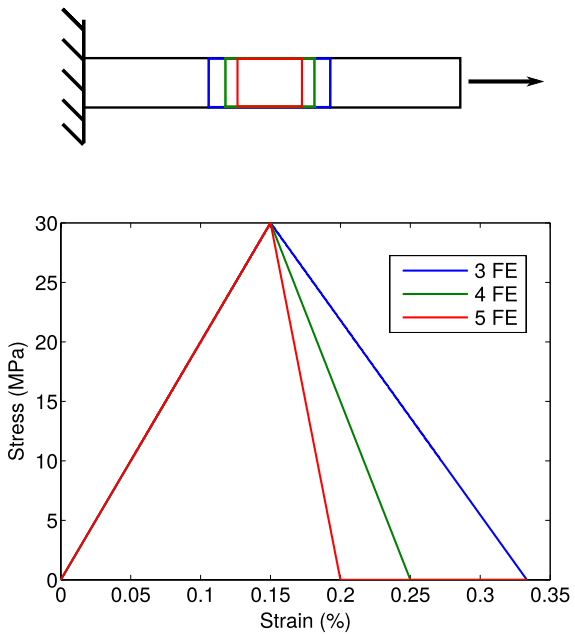

Fig. 13 Finite element simulation of uniaxial tension test. Material parameters: $E = 20000$ MPa, $\sigma_u = 30$ MPa, $K = -3000$ MPa. The result for softening part of the curve is mesh dependent. Namely, smaller the element, the more localized damage and smaller fracture energy leads to more brittle response. (Color figure online)

Another widely published approach to numerically deal with materials which undergo strain localization and softening with pathological dependence on the refinement of the grid is multi-scale modelling [39]. The idea of this approach is to consider the effect of the heterogeneities of the microstructure on the global response of the structure. However, the major question is how to properly transfer the length scales and preserve the energy. There are several multi-scale modelling techniques. The straightforward technique is the direct numerical analysis which is expensive but useful for verification of multi-scale models. Homogenization is another technique in which the heterogeneous material is replaced by an equivalent homogeneous material [39, 40]. In order to achieve this goal, the representative volume element (RVE), which is a micro or meso sub-domain representative for the entire micro or meso structure in an averaged sense, needs to be defined. However, the different sizes of the RVE's in a localized process produce non objective results, which again seems to be the major drawback. Namely, the ongoing question is still how to properly identify the size of the localized zone to obtain the correct failure response. One approach to tackle this problem in homogenization methods is failure zone averaging presented in [39]. Another approach published recently is to model the discrete cracks in softening RVE with embedded strong discontinuities whose formulation easily distinguishes between loading in the damaged zone and unloading in the neighbourhood [41], or when continuum elements with embedded strong discontinuity formulation are used in a standard FE^2 scheme at micro and macro scale [42]. Accurate multi-scale modelling of materials require the use of multi-scale techniques being able to successfully bridge the various scales and to provide the most important effects of lower scales. Multi-scale theories can be found in the literature, even for modelling nano-composite materials and atomistic and molecular systems [43]. However, bridging the scales can be extremely complex and computationally demanding especially when getting to lower nano and atomistic scales. Special software procedures and sometimes code coupling strategies are needed to complete this task [44].

Although methods based on localization limiters and multi-scale homogenization techniques can provide mesh independent softening responses, there is still a question of the true origin of the localized fracture process zone. In order to fully understand it, one has to consider the disorder explicitly through a lot of statistics and to observe the fracture at the atomistic level [35]. Molecular dynamics is a numerical tool developed in the late 1950s for studying physical movements of atoms and molecules. The atoms

Author's personal copy

and molecules interact between each other resulting with a dynamical evolution of the system. The principle of molecular dynamics simulations is to determine the trajectories of atoms by solving Newton's equation of motion. Forces between the particles and their potential energies are calculated using inter-atomic potentials, which represent the crucial ingredient of molecular dynamics simulations. Molecular dynamics simulations are computationally very intensive since the evaluation of the potential as a function of the millions of particles is needed. Another difficulty is the choice of the size of the integration time step which must be small enough to avoid discretization errors. Time steps are usually of the order of 1 femtosecond ($10^{-15}s$).

Despite the heavy computational requirements, molecular dynamics simulations have been successfully applied to provide more insight into the propagation of cracks considering the atomistic aspects of a material [45]. It has been shown that the serious shortcomings of the fracture mechanics related to singularities at the crack tip and the size of the localized zone can be solved by considering the bond breaking between atoms and thus departing from the continuum mechanics towards the atomistic description of fracture. More precisely, it is possible to correctly identify the size of the fracture process zone at the atomistic level. The trajectories of the atoms obtained through Newton's equation of motion can provide the structural, dynamical, thermal and mechanical properties of the system. Molecular dynamics simulations can naturally account for nonlinearities and disorder of the system.

An inter-atomic potential function provides a description of the terms by which the atomic particles in the simulation will interact. One simple two-body inter-atomic potential is Lennard-Jones potential (LJ) used for calculating van der Waals forces in vacuum. Although rather simple, LJ is able to describe a huge variety of material behaviours. Several modifications of the potential have been developed resulting in the possibility to represent both ductile and brittle behaviours. Simulations obtained with LJ potential have shown that stress and strain fields due to a point source force acting on a bidimensional amorphous material result with average stresses and displacement fields which compare well with the predictions from classical isotropic elasticity. However, large stress and strain fluctuations are found near the localized zone which come as a result of intrinsic disorder of amorphous systems [46]. Fracture and damage of silicate glasses and ceramics can be solved by combining two-body and three-body potentials. The two-body interaction accounts for Coulomb interaction due to charge transfer, while three-body potential serve for covalent effects [47]. A significant potential lies in molecular dynamics simulations which can be used to obtain the critical stress intensity factors, fracture toughness or the morphology of fracture surfaces. They also provide a great potential for understanding the mechanical behaviour, crack propagation and failure mechanisms in various materials. Valuable information can be extracted at the crack tip and the surrounding region up to sub-micron length scales, as well as information about the origin of stress heterogeneities which control these mechanisms [45] (Fig. 14). However, such simulations are very complicated and computationally expensive often dealing with millions of atoms. Thus, they are not practical, especially in engineering practice. A more efficient way of considering the above mentioned phenomena which are crucial for failure of real materials and highly influence the failure mechanisms can be obtained through the use of lattice models.

3.2 Lattice Models for Failure at Micro-/Meso-scale

Lattice models, described previously in Sect. 2, may be successfully used for simulations of failure of heterogeneous disordered materials. They can be considered as an alternative to molecular dynamics simulations, but with justification on a larger length scale. Namely, molecular dynamics, as a more fundamental approach, describes the material at the atomistic scale, while lattice models may naturally be used in representing the micro-/meso-scale of quasi-brittle materials like soils, rocks, concrete, ceramics, marl etc. The latter are cemented granulates forming macroscopic solids, where the grains of the material are taken as a large collection of small scale units (atoms and molecules) interacting elastically with each other. Thus one should deal with elastic or plastic equations of motion instead of complicated interatomic potentials [35]. The granular meso or micro structure of such materials naturally agrees with the

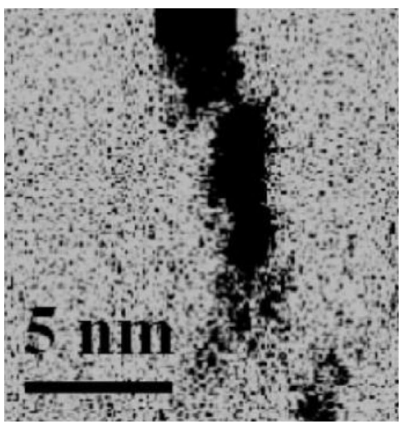

Fig. 14 Snapshot of a molecular dynamics simulation showing the crack and nanopores (*dark*) and atoms (*light*) in an amorphous Si_3N_4 film. Initially the crack propagates straight. Voids in front of the crack coalesce with each other and form a second crack (Taken from [45])

Author's personal copy

framework of lattice models (Fig. 15). As stated in Sect. 2, lattice models are constructed from a collection of lattice nodes which can be regularly of irregularly distributed along the domain. Lattice nodes are connected with lattice elements usually forming a Delaunay triangulation, while each node corresponds to a single grain or particle of the material. Material particles can be represented by Voronoi cells (Figs. 9 and 10), which are dual to Delaunay triangulation, or spheres (alternatively circles in 2D) (Fig. 1b).

An assembly of such micro or meso scale particles, which are cemented and bonded together, form the vast number of quasi brittle materials. In order to bond the particles together, a cohesion force between them is required. This is easily fulfilled with lattice model approach, where lattice elements can represent the cohesive forces between the particles. A significant benefit of the cohesive approach for fracture has already been experienced in the early 1960s by Barenblatt [48] and Dugdale [49] with an introduction of cohesive zone models. The cohesion force in the material results from atomic and molecular bonds at the atomistic scale of the material. The concept of cohesive fracture is regarded as a gradual separation of the surfaces involved in the crack which takes place across an extended crack tip, or cohesive zone, and is resisted by cohesive tractions when material elements are pulled apart. Traction first increases with the separation of surfaces until a maximum value is reached, and then gradually reduces to zero which results in softening behaviour. Thus, it is necessary to describe the traction-displacement curve as a constitutive behaviour of the fracture for full failure application. The area under this curve represents the fracture energy which is a physical parameter and can be obtained experimentally. The greatest advantage of the cohesive approach for fracture is that it bypasses the problem of singularity of the stress at the crack tip and defines the criterion related to the cohesive strength of the material. Moreover, it can consider the dissipative processes in the non-linear localized zone which can spread even to the wider area around the crack. Thus, fracturing of both ductile and brittle materials can be studied with cohesive fractures.

In order to trigger the cohesive fracture, an additional criterion for breaking of the lattice needs to be introduced into the model. Such a breaking rule should reflect the atomistic state of the rupture initiation and one should carefully choose it, taking care about the correct failure mechanism occurring in the observed material. More precisely, the failure criterion on every beam or spring in the domain should be checked to realize if the bond reached its ultimate value. If the failure criterion is reached, the cohesive bond is either removed or undergoes softening (more information on the post failure response is provided in the Sect. 3.5). Mechanical breaking rules can be based on a certain stress criterion, where traction acting on the crack is compared to the ultimate stress value like in cohesive zone models, or even maximum strain criterion. In quasi-brittle materials, stress and strain criteria often pertain to failure modes I, II and III, reflecting the tensile opening or shear sliding (Fig. 12). However, their combination resulting with mixed-mode fracture propagation can also be encountered. Failure due to bending cannot be neglected in some materials (glass for example) and its contribution can also enter the failure rules.

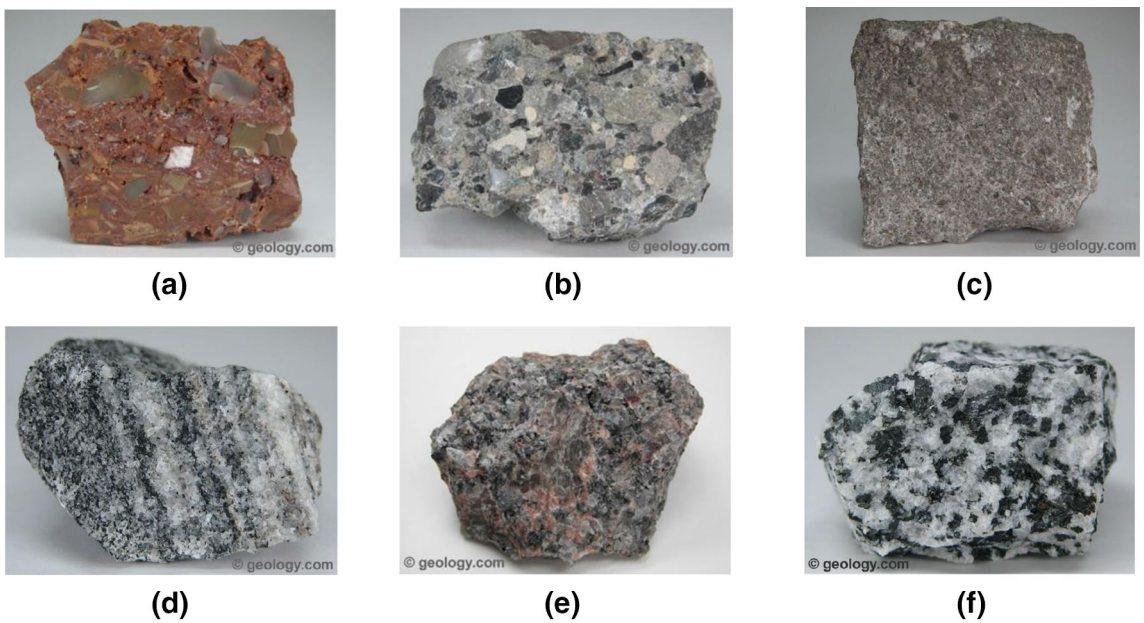

Fig. 15 Grainy structure of different rocks: **a** breccia (sedimentary), **b** conglomerate (sedimentary), **c** limestone (sedimentary), **d** gneiss (metamorphic), **e** granite (igneous), and **f** quartz-diorite (igneous). The size of all of the samples is approximately 5 cm. Taken from [9]

Author's personal copy

Having the failure criterion checked on every lattice element, it is allowed to have many small and sharp cracks which can interact, simultaneously grow or merge together forming dominant larger cracks, like shown in Fig. 16. This represents a significant advantage over models in linear elastic fracture mechanics where multiple cracks invoke many problems. Moreover, one does not need to think about the definition of complex crack geometries, which especially provide a lot of difficulties in 3D. Alternatively, it is also possible to enforce the single crack by knowing the connectivity between the elements and allowing to break only the elements in the closest neighbourhood of the crack.

Lattice models possess a natural ability for introduction of disorder. This represents a huge benefit since disorder has an important effect on the breaking process. Disorder in lattice models usually pertains to meso-scale heterogeneities of some composite material or can contain the effects of micro structural deviations. In many lattice models (which simulate the meso-scale structure), disorder pertains to local densities, elastic modulus or material strength. Namely, each cohesive link in the lattice is represented by a certain constitutive law which describes the material behaviour (Fig. 17). Perfectly brittle failure in Fig. 17a is characterized by elastic behaviour with given modulus of elasticity and failure threshold. One could implement the presence of disorder by applying the different values for threshold or modulus of elasticity by some random distribution. This leads to a different behaviour of each bond reflecting the disorder at microscopic scales. Moreover, if one wants to obtain more ductile behaviour in each bond, the constitutive law with softening behaviour could be implemented (Fig. 17b). The variation is possible in this case as well by applying the different values of fracture energies G_f for softening.

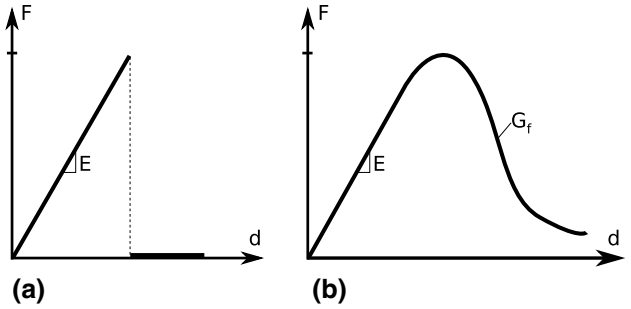

Fig. 17 Constitutive behaviour of each cohesive link in the force-displacement coordinate system: **a** perfectly brittle failure **b** failure with softening

A vast number of lattice model applications can be found in meso-scale simulations of composite materials like concrete or rocks. The multi-phase structure of composites is clearly recognizable at the meso-scale, where concrete is composed of coarse aggregates bonded together with cement. Each phase is characterized by different material properties which can be applied to different lattice elements like shown in Fig. 18. Coarse aggregates as spherical inclusions can be generated with the Gibbs point process, taking into account both prescribed density and inclusion radius [6]. Other cumulative distribution functions can be used to randomly place the aggregates inside the observed domain [28]. It is also possible to estimate the critical size of the aggregates where only larger ones are modelled by positioning them inside the domain, while the heterogeneities produced by finer ones can be considered by some distributions. The model can also account for interface elements which appear between the two phases, resulting with a three phase material. Some papers refer to such observational scale as a mini-scale [12]. Two phases can

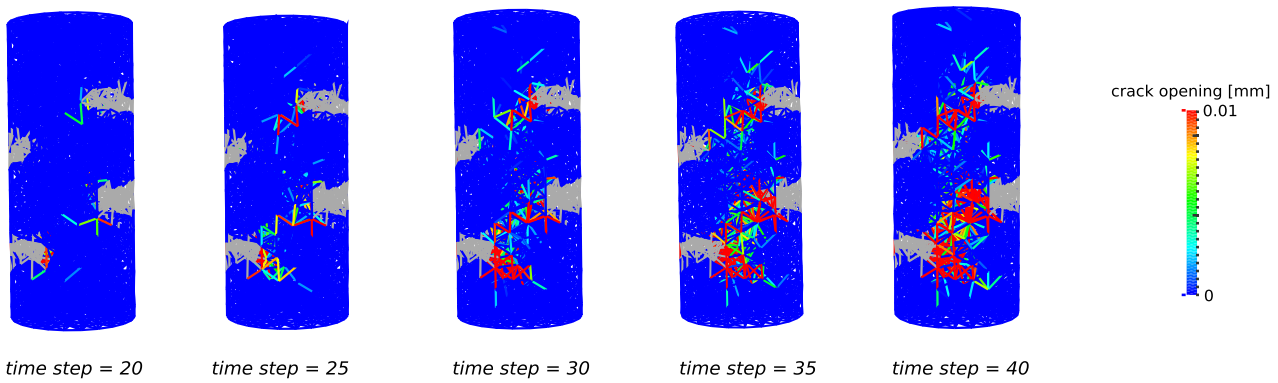

Fig. 16 A result of the 3D lattice model simulation presented in [9]. Cylindrical rock specimen is constructed out of beams as the cohesive links. The *grey coloured* beams are intentionally positioned at the opposite ends of the specimen representing the weak phase of the material which triggers the cracks. Breaking rules on the cohesive links allow to simulate simultaneously many cracks in the domain which can propagate, coalesce and merge. (Color figure online)

Author's personal copy

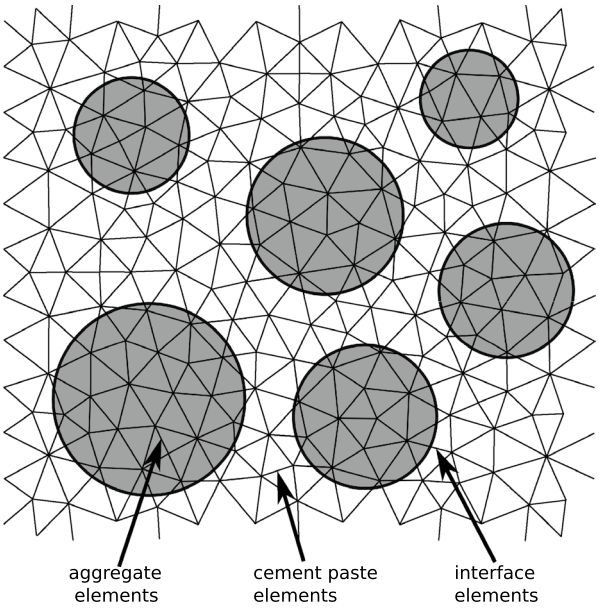

Fig. 18 Multi-phase representation of concrete. Material parameters of the lattice elements falling into cylindrical inclusions correspond to aggregates, while the ones outside correspond to cement. In addition, it is possible to consider the interface elements

be easily identified at the meso-scale of rocks, where one phase could represent the intact rock while the second one accounts for pre-existing defects [8, 9].

Such favourable properties led to the vast usage of lattice elements in simulations of concrete micro-/meso-scale. Some of the notable lattice model applications to concrete are presented in papers of Schlangen and van Mier [4, 5], Schlangen and Garboczi [2], Chang et al [22], Lilliu and van Mier [50], Karihaloo et al [23], or in some recent papers by Vassaux et al [10, 11], Grassl et al [28, 29], Cusatis et al [12, 13, 21].

3.3 Lattice Models for Failure at Macro-scale

We have shown that the concept of lattice models comes as a natural choice for simulations at finer scales, especially because the material structure is discontinuous and often resembles a lattice. However, despite their natural applicability at finer scales, lattice models may also be used to simulate the failure of solids at a macro-scale, where the lattice structure represents an initially continuous material in which discontinuities develop during loading. The failure of solids with discontinuity propagations has been a major topic of research in the last decades and still represents a task which is not easily tackled. This is generally due to occurrence of instabilities in numerical algorithms upon reaching softening behaviour in material caused by crack propagation, and geometric representations of cracks and

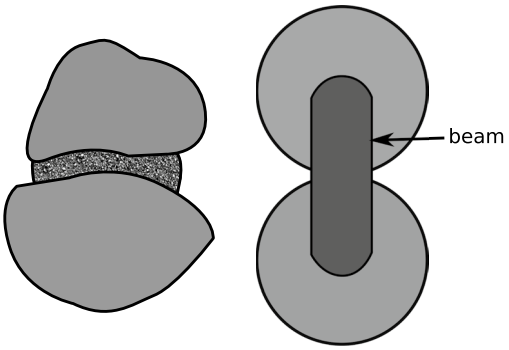

Fig. 19 Two aggregates idealized with spherical particles kept together by a beam as a cohesive link in cohesive DEM

discontinuities, especially when many of them are present in the domain. The enhanced finite element methods for handling discontinuities inside continuum solid elements, like X-FEM [51–53] and FEM with embedded strong discontinuities (ED-FEM) [54–58], have been developed to solve the problem of failing solids. However, X-FEM and ED-FEM require the tracking algorithms for the discontinuities which are still very challenging in 3D. On the contrary, lattice models do not require tracking algorithms, but cracks occur as a result of breaking the cohesive links between the cells and thus represent a propagating discontinuities in a homogeneous solid. For example, simulations of macro-scale structures with reinforced concrete incorporating the reinforcement into the lattice structure are conducted in [59, 60]. Failure of homogeneous solids with reinforced fiber inclusions can be found in [24, 26].

3.4 Similarity Between the Lattice Element Models and Discrete Element Models

It is worth noting that the concept of lattice elements can be very similar to discrete element method (DEM) with cohesion, in which rigid particles are kept together by cohesive forces as well. The discrete element method is usually applied to large displacement problems of granular media, while each particle is governed by equations of motion during the simulation [61]. Moreover, the particles are interacting between each other and the collision between the particles with contact is involved during the simulation. In the case of standard discrete element method, one can compute only the contact forces between the particles and cannot determine the stress distribution at the particle scale. In the case of cohesive DEM, the cohesive bonds can be modelled like in lattice models, with beams (Fig. 19). The cohesive DEM approach has already been used for modelling cohesive materials, like concrete, asphalt, hard rock and cemented sands [62–65]. Cohesive DEM approach

Author's personal copy

still uses the contact law for the interaction of particles that were debonded during the simulation [66].

Lattice models find their main purpose in simulating small displacement problems especially with localized failure resulting in cracking mechanisms where stress concentrations and its redistribution upon cracking is more important. This usually occurs under quasi-static conditions, which is in contrast with DEM where dynamic equations of motion of each particle are solved. In most quasi-static lattice models, rigid particles are not programmed for collision with contact detection and interaction like in DEM, mostly because there are no larger movements and significant changes in particle topology. The important aspect is to capture the crack propagation between the particles while the particle connectivity is preserved from the beginning. This is suitable for tension and shear tests where no major collisions of the loose particles of the material are expected. The main role of the particles is in computing the stiffness parameters where larger particles bring more stiffness to their cohesive link. The results of the simulations are often plotted on the frame or lattice structure showing the stresses in the cohesive lattice elements, while the particles are not necessarily plotted.

However, lattice models have been recently enhanced to capture the collision between the unbonded particles with implemented contact algorithms [10–13]. Such models are very similar to cohesive DEM models with contact. The model presented in [10, 11] proved that the implementation of contact and collision between the particles even under quasi-static loading conditions where no significant change in topology appears, brings the ability to reliably simulate compression tests, where detachment of the material occurs with additional sliding and fragmentation between the broken parts.

Despite being applied mostly to quasi-static loading conditions, the lattice elements can also be used for simulation of dynamic problems as well. D'Addetta and coauthors [67, 68] developed the discrete lattice model with Voronoi cells as randomly shaped convex polygons which represents material grains, and where both static and dynamic equations of motion are solved. The wide applicability of this model is ranging from the quasi-static uniaxial loading and shearing of geomaterials to the dynamic fragmentation due to explosion, impact and collision of solids. The lattice model presented in [69, 70] is developed for dynamic problems with contact interaction and detection between the unbonded Voronoi cells which are kept together prior to failure by large displacement geometrically exact shear deformable beams as cohesive forces. The model is suitable for impact simulations in which cracks occur as a result of large movements of the rigid Voronoi particles.

3.5 Dealing with Post-peak Softening Response

Occurrence of cracks leads to redistribution of stresses to the surrounding area. Since the stresses are redistributed, new cracks may form and continue to propagate. If the stored elastic energy is larger that the fracture energy already used in crack forming, strong drops in the force-displacement curve can happen. This can easily lead to a brittle response of the structure. Additionally, snap-back or snap-through responses in the load-displacement curves often occur when complex failure mechanisms are present. The softening part of the load-displacement curve comes as a result of the failure of the bonds, and it can provide numerical difficulties and instabilities in nonlinear incremental-iterative analysis due to negative stiffness terms. Moreover, complex situations like unloading and reloading of the already failed elements bring even more challenges for integration schemes.

In order to trace the global softening curve all the way down, one should consider an incremental-iterative procedure with arc-length or displacement control of the nonlinear system.In order to avoid possible divergence in the solution, most lattice models uses a sequentially linear scheme instead of nonlinear incremental-iterative scheme. One such algorithm, called the saw-tooth algorithm, is well explained in [71].

In sequentially linear algorithms, one needs to solve the system and check if the failure criterion in each element is satisfied. If yes, the crack is starting to propagate and internal boundary conditions related to the crack should be changed. Namely, in a brittle failure like shown in Fig. 17a, the element is removed from the mesh or its modulus of elasticity is set to zero. Consequently, the system is restarted from the origin and solved again in a completely linear way with previously modified parameters for the crack. Failure criteria for the recently obtained solution need to be checked again to decide which bonds are eligible to break in the current step. The repetition of such process represents the sequentially linear analysis in which solving of the system of linear equations and change of internal boundary conditions are repeated as many times as bonds are broken. The advantage of such approach is that the solution is always stable and simple, while the stiffness matrix does not contain negative stiffness terms which occur in a nonlinear incremental-iterative analysis with stress reduction. Thus, one does not worry about the convergence issues since only linear analysis is performed in a sequential manner. The disadvantage of the complete removal of lattice elements is that sudden release of the stress dropping to zero in failed elements usually leads to a very brittle failure, and global fracture energy can be easily underestimated with respect to the experiment.

Author's personal copy

Since the global response depends on the way how the stiffness of the broken elements is reduced, one needs to consider the gradual decrease in stiffness leading to softening behaviour (Fig. 17b), instead of just instantly reducing it to zero. This is possible by reducing the strength from f_t to zero in n steps while the corresponding reduced Youngs modulus E_i is subsequently computed from the envelope curve (Fig. 20) [71].

Although the sequentially linear algorithm is stable and approximates a nonlinear curve without the use of iterative solvers, it suffers from the mesh objectivity problem. Namely, the issue of the size of the localized zone which has already been addressed previously, is still present. Refinement of the mesh produces narrower localized zone and more pronounced underestimation of the dissipated energy. In order to overcome this issue, regularization schemes have been developed. Some of them pertain to increasing of ductility of cohesive bonds to obtain the correct macroscopic response which corresponds to a nonlinear reference curve [71]. However, a unique representation of dissipated fracture energy independent of the size of the lattice elements is needed. The embedded discontinuity approach which acts as a localization limiter has been recently applied with lattice element models to overcome the mesh dependency related to the size of the localized zone.

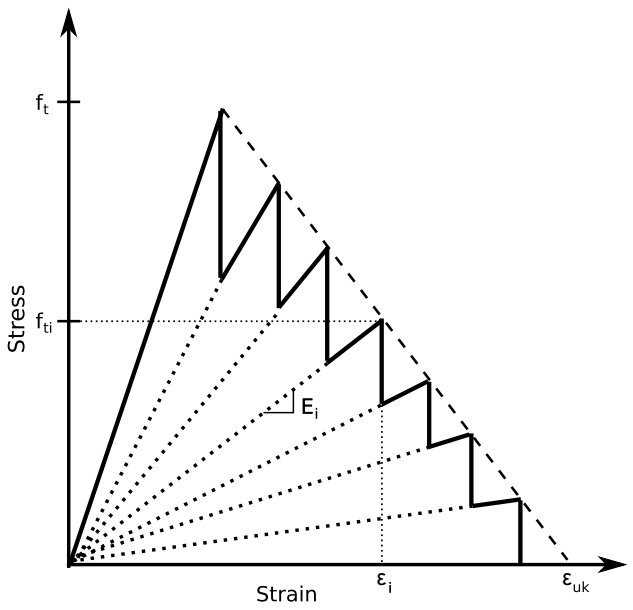

Fig. 20 Reduction of strength f_t to zero of each cohesive link in n steps by sequentially linear algorithm

4 Embedded Strong Discontinuity in Lattice Element Models

The importance of the size of the localized zone around the crack has been noticed in failure of various materials. Inside this zone, plastic or damage dissipative mechanisms occurs influencing the final failure. This phenomenon is even confirmed by using various models. Namely, in linear elastic fracture mechanics, the amount of such dissipation and the size of the zone around the crack tip play a key role in failure criteria. In standard finite elements, the size of the mesh is related to the size of the localized zone, influencing the dissipation. The same happens with lattice element models. Various methods and approaches have been developed to stabilize the size of this zone by producing mesh independent results.

One of the approaches which can successfully bypass the issue of the mesh size related to size of the localized zone is the embedded discontinuity approach. It has already been mentioned in Sect. 3.2, in the context of solid elements with propagating discontinuities. More precisely, it is the embedded strong discontinuity, or discontinuity in the displacement field, which is capable of providing mesh independent response. The reason for this is that the discontinuity always remains localized inside the element by using the displacement jump, usually represented by the Heaviside function. The main idea of the approach is that by providing a fracture energy as an input, which is a physical parameter obtained from an experiment, results remain mesh independent. This approach can be observed as a localization limiter that enhances the classical continuum mechanics theoretical formulation by admitting discontinuities in the displacement field [72, 73]. The numerical implementation of the discontinuity requires a modification of the standard finite element procedure, which is similar to the method of incompatible modes [74, 75].

The embedded strong discontinuity concept has been firstly used in lattice models, with truss bars as lattice elements [6, 7], transmitting normal force and accounting for softening failure of the truss bar. Moreover, embedded weak discontinuity is also present in this formulation, representing the jump in the strain field, which serves for interface elements in concrete where two materials are provided inside one element. The detailed finite element implementation of embedded strong and weak discontinuity into truss bar can be found in [36, 76]. Since the failure of quasi-brittle materials requires the shear failure mechanism, the Timoshenko beam as lattice element is taken to construct the lattice model in 2D [8] and 3D [9] setting. Timoshenko beam with embedded strong discontinuity formulation in rotation can be found in [77], or in rotation and transversal beam direction in [78].

Author's personal copy

4.1 2D Lattice Model with Enhanced Timoshenko Beams as Lattice Elements

A lattice model with Timoshenko beams as cohesive links, with embedded strong discontinuity, is presented in [8] (Fig. 21). In order to provide the beam failure modes, the Timoshenko beam is enriched with kinematic enhancements in its longitudinal and transversal directions, resulting with discontinuities in normal force and shear force, respectively.

The embedded strong discontinuity in the beam longitudinal local direction enable the grain dilation due to mode I or tensile failure mode. Timoshenko beam allows to account for pronounced shear effects which is used here for representing the failure in mode II (shear sliding along the grains) adding the corresponding displacement or strong discontinuity in the transversal local direction (Fig. 22). Thus, a set of two failure mechanisms provides the possibility for representing a complex crack evolution, while localization is stabilized inside beam elements and remains mesh independent.

4.2 Kinematics of Enhanced Timoshenko Beam Element

In order to obtain a heterogeneous displacement field, kinematics of the Timoshenko beam needs to be enhanced. More precisely, it is the axial and shear strains which need to be enhanced to provide mode I and mode II failure. One can start from standard kinematics of a geometrically linear

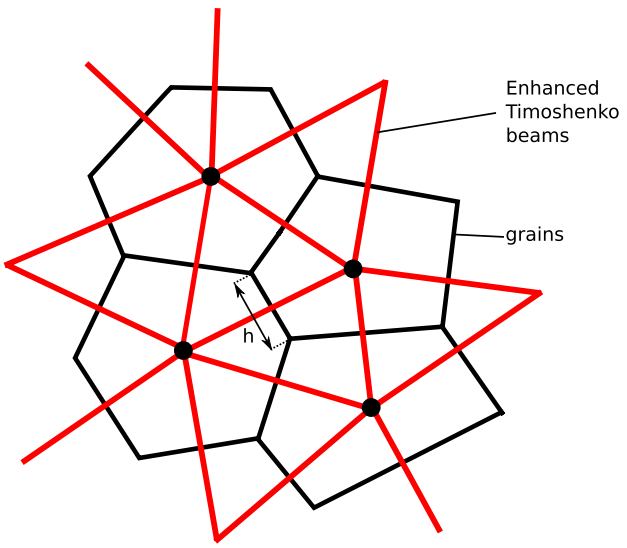

Fig. 21 Lattice model constructed from enhanced Timoshenko beams as cohesive links and Voronoi scaling which serves for computation of lattice parameters as elaborated in Sect. 2.1.2. (Color figure online)

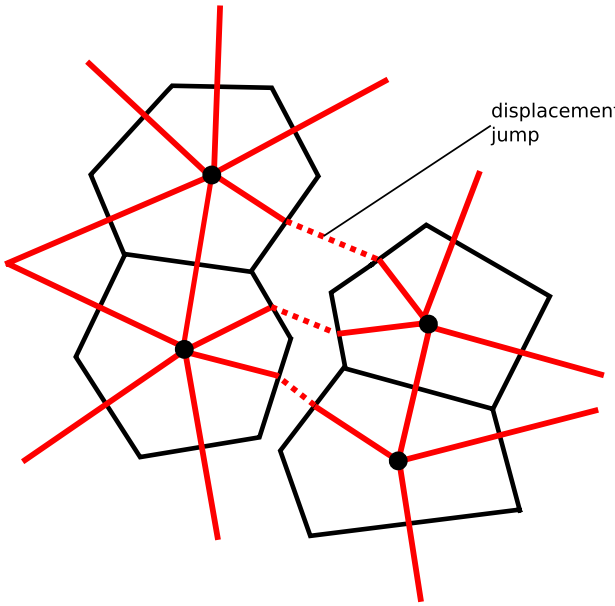

Fig. 22 The strong discontinuity propagation between the Voronoi cells invokes the enhanced kinematics activation. (Color figure online)

Timoshenko beam finite element of length l_e and cross section A to obtain the strain measures $\boldsymbol{\epsilon}$

$$\boldsymbol{\epsilon}(x) = \begin{bmatrix} \epsilon(x) = \frac{du}{dx} \\ \gamma(x) = \frac{dv}{dx} - \theta \\ \kappa(x) = \frac{d\theta}{dx} \end{bmatrix} \tag{26}$$

where $\mathbf{d} = [u \;\; v \;\; \theta]^T$ is the generalized displacement vector with its longitudinal displacement, transversal displacement and rotation. The strong form of Timoshenko beam can be recast in terms of stress resultants

$$\begin{aligned} &\tfrac{dN}{dx} + f(x) = 0 \\ &\tfrac{dT}{dx} + q(x) = 0 \\ &\tfrac{dM}{dx} + T(x) + m(x) = 0 \end{aligned} \tag{27}$$

where $\boldsymbol{\sigma} = [N \;\; T \;\; M]^T$ represents the stress resultant vector and $\mathbf{f} = [f \;\; q \;\; m]^T$ is the distributed load vector. The enhanced displacement field with discontinuity needs to be constructed out of regular and singular parts, where the latter can be represented as a product of the Heaviside function and displacement jump. The enhanced displacement fields can then be written as

$$\mathbf{d}(x) = \overline{\mathbf{d}}(x) + \boldsymbol{\alpha} H_{x_c} = \begin{bmatrix} \overline{u}(x) \\ \overline{v}(x) \\ \overline{\theta}(x) \end{bmatrix} + \begin{bmatrix} \alpha_u \\ \alpha_v \\ 0 \end{bmatrix} H_{x_c} \tag{28}$$

where enhancements pertain here to longitudinal and transversal displacements, while rotation remains linear.

Author's personal copy

$\boldsymbol{\alpha} = [\alpha_u \;\; \alpha_v \;\; 0]$ is the discontinuity related parameter which is similar to incompatible mode parameter and H_{x_c} is the Heaviside function defined by $H_{x_c}(x) = 0$ for $x \leq x_c$ and $H_{x_c}(x) = 1$ for $x > x_c$. The non-regular displacement field produces the strain field which is enhanced through the Dirac delta resulting from the discontinuous displacement field

$$\boldsymbol{\epsilon}(x) = \overline{\boldsymbol{\epsilon}}(x) + \boldsymbol{\alpha}\delta_{x_c} = \begin{bmatrix} \overline{\epsilon}(x) \\ \overline{\gamma}(x) \\ \overline{\kappa}(x) \end{bmatrix} + \begin{bmatrix} \alpha_u \\ \alpha_v \\ 0 \end{bmatrix} \delta_{x_c} \tag{29}$$

In order to obtain the interpolation function for discontinuity in displacement fields which cancels its contribution on the boundaries, one can rewrite enhanced displacement fields from Eq. (28) with the function N_2

$$\begin{aligned} u(x) &= \overline{u}(x) + \alpha_u N_2(x) + \alpha_u (H_{x_c} - N_2(x)) \\ v(x) &= \overline{v}(x) + \alpha_v N_2(x) + \alpha_v (H_{x_c} - N_2(x)) \end{aligned} \tag{30}$$

where $\{N_1(x) = 1 - x/l_e,\; N_2(x) = x/l_e\}$ are the standard linear interpolation functions, and their derivatives are $\{B_1^d(x) = -1/l_e, B_2^d(x) = 1/l_e\}$. The second part of (30) pertains to the discontinuity contribution producing the additional interpolation function $M(x)$ (Fig. 23)

$$M(x) = \begin{cases} -\frac{x}{l_e}; \; x \in [0, x_c\rangle \\ 1 - \frac{x}{l_e}; \; x \in \langle x_c, l_e] \end{cases}. \tag{31}$$

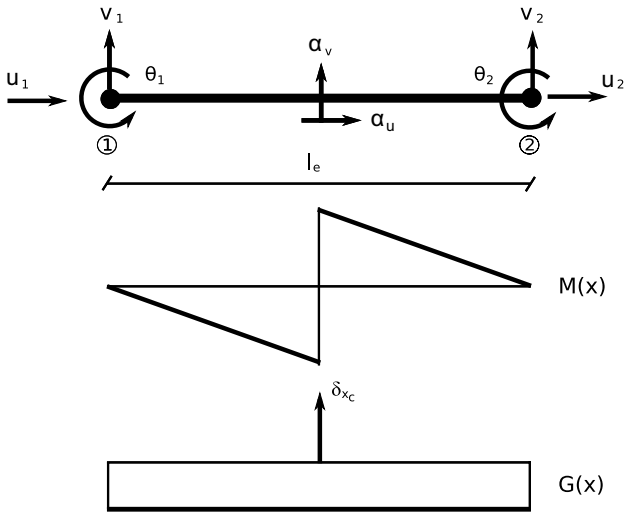

Fig. 23 Timoshenko beam with standard degrees of freedom and additional ones related to jumps in the displacement fields. $M(x)$ and $G(x)$ are the discontinuity related additional interpolation functions

Finally, the discontinuous displacement fields can be interpolated as

$$\begin{aligned} u(x) &= \sum_{a=1}^{2} N_a(x) u_a + M(x)\alpha_u \\ v(x) &= \sum_{a=1}^{2} N_a(x) v_a + M(x)\alpha_v \\ \theta(x) &= \sum_{a=1}^{2} N_a(x)\theta_a. \end{aligned} \tag{32}$$

This formulation, cancelling the contribution of incompatible mode parameter on the element boundary in the regular part of the equation, represents the embedded strong discontinuity. It will later provide the possibility of avoiding the additional global unknowns, since the discontinuity parameter will be computed locally inside the element. The enhanced strain field can be obtained from the enhanced displacement field from Eq. (32) resulting in

$$\begin{aligned} \epsilon(x) &= \sum_{a=1}^{2} B_a(x) u_a + G(x)\alpha_u \\ \gamma(x) &= \sum_{a=1}^{2} \left(B_a(x) v_a - N_a(x)\theta_a \right) + G(x)\alpha_v \\ \kappa(x) &= \sum_{a=1}^{2} B_a(x)\theta_a \end{aligned} \tag{33}$$

where $G(x)$ is the derivative of $M(x)$

$$G(x) = \overline{G} + \delta_{x_c} = -\frac{1}{l_e} + \delta_{x_c}, \quad x \in [0, l_e]. \tag{34}$$

4.3 The Enhanced Weak Form

The enhanced strain field from Eq. (33) can be written in its generalized form

$$\boldsymbol{\epsilon} = \mathbf{B}\mathbf{d} + \mathbf{G}\boldsymbol{\alpha}, \tag{35}$$

where $\mathbf{B}$ is the standard strain displacement matrix for the Timoshenko beam

$$\mathbf{B} = \begin{bmatrix} B_1 & 0 & 0 & B_2 & 0 & 0 \\ 0 & B_1 & -N_1 & 0 & B_2 & -N_2 \\ 0 & 0 & B_1 & 0 & 0 & B_2 \end{bmatrix} \tag{36}$$

and $\mathbf{G}$ is the matrix of discontinuity related functions G. The virtual strains can be interpolated in the same manner as the real strains

$$\delta\boldsymbol{\epsilon} = \mathbf{B}\delta\mathbf{d} + \mathbf{G}\delta\boldsymbol{\alpha} \tag{37}$$

Author's personal copy

where $\delta\mathbf{d}$ and $\delta\boldsymbol{\alpha}$ denote the nodal virtual generalized displacement and virtual displacement jumps. The only difference in real and virtual strain fields concerns the modified enhanced contribution $\tilde{\mathbf{G}}$. Namely, it is necessary to enforce the orthogonality between enhanced strain and constant stress within the element which will fulfil the patch test condition as already shown for the method of incompatible modes in [75]

$$\tilde{\mathbf{G}} = \mathbf{G} - \frac{1}{l_e}\int_0^{l_e} \mathbf{G}dx. \tag{38}$$

When the interface is positioned in the middle of element, condition (38) is automatically verified and $\tilde{\mathbf{G}}$ remains the same as $\mathbf{G}$. It should be noted that $\mathbf{G}$ contains the enhanced discontinuity function G which can be decomposed into regular part $\overline{G}$ and singular part holding the Dirac delta function δ_{x_c}. The final work of internal forces upon introducing the enhanced strain and virtual strain fields results with

$$G^{int} = \int_{l_e} (\mathbf{B}^d\delta\mathbf{d})^T\boldsymbol{\sigma}dx + \underbrace{\int_{l_e} \delta\boldsymbol{\alpha}^T(\overline{\mathbf{G}} + \delta_{x_c})\boldsymbol{\sigma}dx}_{\mathrm{h(e)=0}}. \tag{39}$$

The standard internal force vector and the local residual vector due to discontinuity result from Eq. (39)

$$\begin{aligned}\mathbf{F}^{int} &= \textstyle\int_0^{l_e} \mathbf{B}^{d,T}\boldsymbol{\sigma}dx\\ \mathbf{h}^{(e)} &= \textstyle\int_0^{l_e} (\overline{\mathbf{G}} + \delta_{x_c})\boldsymbol{\sigma}dx.\end{aligned} \tag{40}$$

If the local residual $\mathbf{h}^{(e)}$ from Eq. (40) is reduced to zero, the vector $\mathbf{t} = \int_0^{l_e} \delta_{x_c}\boldsymbol{\sigma}dx$ of the internal forces at the discontinuity can be obtained through the regular part of the enhanced local function

$$\mathbf{t} = -\int_0^{l_e} \overline{\mathbf{G}}\boldsymbol{\sigma}dx, \quad \mathbf{t} = (t_u, t_v, 0)^T \tag{41}$$

4.4 Constitutive Model

The constitutive model defined in [8] is classical elastoplasticity where total regular strains can be additively decomposed into elastic $\overline{\epsilon}^e$ and plastic components $\overline{\epsilon}^p$ with additional contribution $\overline{\overline{\epsilon}}$ from the singular part which is related to discontinuity opening. Thus, the total strain fields which contain regular and singular components can be written

$$\begin{aligned}\epsilon &= \overline{\epsilon} + \overline{\overline{\epsilon}} = \overline{\epsilon}^e + \overline{\epsilon}^p + \overline{\overline{\epsilon}}\\ \gamma &= \overline{\gamma} + \overline{\overline{\gamma}} = \overline{\gamma}^e + \overline{\gamma}^p + \overline{\overline{\gamma}}\end{aligned} \tag{42}$$

The failure criteria related to discontinuity opening can be defined with failure functions

$$\begin{aligned}\overline{\overline{\Phi}}_u\left(t_u, \overline{\overline{q}}_u\right) &= t_u - \left(N_u - \overline{\overline{q}}_u\right) \le 0\\ \overline{\overline{\Phi}}_v\left(t_v, \overline{\overline{q}}_v\right) &= |t_v| - \left(T_u - \overline{\overline{q}}_v\right) \le 0\end{aligned} \tag{43}$$

where N_u, T_u are the ultimate capacity forces and $\overline{\overline{q}}_u$, $\overline{\overline{q}}_v$ are stress-like softening variables which increase with exponential softening law

$$\begin{aligned}\overline{\overline{q}}_u &= N_u\left(1 - exp\left(-\overline{\overline{\xi}}_u\frac{N_u}{G_{f,u}}\right)\right)\\ \overline{\overline{q}}_v &= T_u\left(1 - exp\left(-\overline{\overline{\xi}}_v\frac{V_u}{G_{f,v}}\right)\right).\end{aligned} \tag{44}$$

and t_u, t_v are traction forces at the discontinuity obtained from equilibrium equations (41).

4.5 The Local Algorithm

This is an element-wise algorithm, similar to the standard return mapping algorithm in plasticity, performed in beam longitudinal and transversal direction with its ultimate goal of computing the internal variables related to discontinuity. After computing the internal variables locally, the global solution procedure can be performed.

We will assume to be given the best iterative value of displacements $u^{(i)}_{n+1}$ and $v^{(i)}_{n+1}$ for which we can obtain the trial value of the traction force

$$\begin{aligned}t^{trial}_{u,n+1} &= -\int_0^{l_e} \overline{G}\left[EA\left(\sum_{a=1}^{2} B_a u^{(i)}_{a,n+1} + \overline{G}\alpha_{u,n}\right)\right]\\ t^{trial}_{v,n+1} &= -\int_0^{l_e} \overline{G}\left[GA\left(\sum_{a=1}^{2} B_a v^{(i)}_{a,n+1}\right.\right.\\ &\quad \left.\left. - \sum_{a=1}^{2} N_a\theta^{(i)}_{a,n+1} + \overline{G}\alpha_{v,n}\right)\right]\end{aligned} \tag{45}$$

where $\alpha_{u,n}$, $\alpha_{v,n}$ are the discontinuity parameters at the previously converged time step for softening plastic deformation. The trial values of failure functions are calculated next

$$\begin{aligned}\overline{\overline{\Phi}}^{trial}_{u,n+1} &= t^{trial}_{u,n+1} - \left(N_u - \overline{\overline{q}}_{u,n}\right),\\ \overline{\overline{\Phi}}^{trial}_{v,n+1} &= \left|t^{trial}_{v,n+1}\right| - \left(V_u - \overline{\overline{q}}_{v,n}\right)\end{aligned} \tag{46}$$

with $\overline{\overline{q}}_{u,n}$ and $\overline{\overline{q}}_{v,n}$ defined in (44). If the trial values of the failure functions are negative or zero, the elastic trial step is accepted for final, with no modification of the plastic strain from the previous time step

$$\begin{aligned}\alpha_{u,n+1} &= \alpha_{u,n};\ \overline{\overline{\xi}}_{u,n+1} = \overline{\overline{\xi}}_{u,n},\\ \alpha_{v,n+1} &= \alpha_{v,n};\ \overline{\overline{\xi}}_{v,n+1} = \overline{\overline{\xi}}_{v,n}\end{aligned} \tag{47}$$

The plastic softening parameter will remain intact, while the traction force change due to displacement increment.

Author's personal copy

On the other hand, if the trial values of failure functions are positive, the current step is in the softening plasticity and there is a need to modify the elastic strain and internal variables $\alpha_{u,n}$, $\alpha_{v,n}$ in order to re-establish the plastic admissibility at the discontinuity. The internal softening plasticity variables ought to be updated by using evolution equations

$$\begin{aligned}\alpha_{u,n+1} &= \alpha_{u,n} + \overline{\overline{\lambda}}_{u,n+1} sign\left(t^{trial}_{u,n+1}\right)\\ \alpha_{v,n+1} &= \alpha_{v,n} + \overline{\overline{\lambda}}_{v,n+1} sign\left(t^{trial}_{v,n+1}\right)\end{aligned} \tag{48}$$

and

$$\begin{aligned}\overline{\overline{\xi}}_{u,n+1} &= \overline{\overline{\xi}}_{u,n} + \overline{\overline{\lambda}}_{u,n+1}\\ \overline{\overline{\xi}}_{v,n+1} &= \overline{\overline{\xi}}_{v,n} + \overline{\overline{\lambda}}_{v,n+1}\end{aligned} \tag{49}$$

where $\overline{\overline{\lambda}}_{u,n+1}$, $\overline{\overline{\lambda}}_{v,n+1}$ are softening plastic multipliers. The value of the plastic multiplier is determined from the conditions $\overline{\Phi}_{u,n+1} \le tol$ and $\overline{\Phi}_{v,n+1} \le tol$ and the solutions of nonlinear equations are obtained iteratively using the Newton-Raphson method

$$\begin{aligned}\overline{\overline{\Phi}}_{u,n+1} &= \overline{\overline{\Phi}}^{trial}_{u,n+1} + \left(\overline{\overline{q}}_{u,n+1} - \overline{\overline{q}}_{u,n}\right) + EA\overline{G}\overline{\overline{\lambda}}_{u,n+1} \le tol\\ \overline{\overline{\Phi}}_{v,n+1} &= \overline{\overline{\Phi}}^{trial}_{v,n+1} + \left(\overline{\overline{q}}_{v,n+1} - \overline{\overline{q}}_{v,n}\right) + GA\overline{G}\overline{\overline{\lambda}}_{v,n+1} \le tol\end{aligned} \tag{50}$$

In the plastic softening step, the traction forces are produced by a change of discontinuity parameters α_u and α_v.

4.6 Global Procedure

The global solution should be performed in order to provide new iterative values of nodal displacements upon completing the local phase in which internal variables are computed. The set of global equilibrium equations is checked with previously computed internal forces

$$\left\| A_{e=1}^{n_{el}} (f^{int,e,(i)} - f^{ext,e}) < tol \right\| \tag{51}$$

If the convergence is satisfied, a new pseudo-time incremental step is performed. If it is not satisfied, a new iterative sweep is performed. From the incremental-iterative finite element procedure we obtain the new values of nodal displacement. Contribution of one single element, denoted with superscript (e), can be stated as

$$\begin{bmatrix} K^{(e)} & F^{(e)} \\ F^{(e),T} & H^{(e)} \end{bmatrix}^{(i)}_{n+1} \begin{pmatrix} \Delta\mathbf{d}^{(e),(i)}_{n+1} \\ \Delta\boldsymbol{\alpha}^{(e),(i)}_{n+1} \end{pmatrix} = \begin{pmatrix} \mathbf{f}^{ext,(e)}_{n+1} - \mathbf{f}^{int,(e),(i)}_{n+1} \\ \mathbf{h}^{(e),(i)}_{n+1} \end{pmatrix}. \tag{52}$$

The superscript (i) denotes the iteration counter. The parts of the element stiffness matrix are

$$\begin{aligned} K^{(e),(i)}_{n+1} &= \left(\frac{\partial \mathbf{f}^{int,(e)}}{\partial \mathbf{d}^{(e)}}\right)^{(i)}_{n+1} = \int_0^{l^e} \mathbf{B}^T \mathbf{C}_{n+1} \mathbf{B} dx \\ F^{(e),(i)}_{n+1} &= \left(\frac{\partial \mathbf{f}^{int,(e)}}{\partial \boldsymbol{\alpha}^{(e)}}\right)^{(i)}_{n+1} = \int_0^{l^e} \mathbf{B}^T \mathbf{C}_{n+1} \mathbf{G} dx \\ H^{(e),(i)}_{n+1} &= \left(\frac{\partial \mathbf{h}^{(e)}}{\partial \boldsymbol{\alpha}^{(e)}}\right)^{(i)}_{n+1} = \int_0^{l^e} \mathbf{G}^T \mathbf{C}_{n+1} \mathbf{G} dx + \mathbf{K}_s \end{aligned} \tag{53}$$

where

$$\mathbf{C}_{n+1} = \begin{bmatrix} C^{(u)}_{n+1} & 0 & 0 \\ 0 & C^{(v)}_{n+1} & 0 \\ 0 & 0 & EI \end{bmatrix}, \mathbf{G} = \begin{bmatrix} \overline{G} & 0 & 0 \\ 0 & \overline{G} & 0 \\ 0 & 0 & 0 \end{bmatrix} \tag{54}$$

The local equilibrium is automatically satisfied by using the traction computed with Eq. (41).

The static condensation of the matrix allows us to form the final stiffness matrix for the element contribution to the FE assembly

$$A_{e=1}^{n_{el}} \left(\widehat{K}^{(e),(i)}_{n+1} \Delta\mathbf{d}^{(e),(i)}_{n+1} \right) = A_{e=1}^{n_{el}} \left(\mathbf{f}^{ext,(e)} - \mathbf{f}^{int,(e),(i)} \right) \tag{55}$$

where

$$\widehat{K}^{(e),(i)}_{n+1} = K^{(e),(i)}_{n+1} - F^{(e),(i)}_{n+1} \left(H^{(e),(i)}_{n+1} \right)^{-1} F^{(e),(i),T}_{n+1} \tag{56}$$

The solution of the global system (51) provides the next iterative update $\Delta\mathbf{d}^{(e),(i)}_{n+1}$. Matrix $\mathbf{K}_s$ contains consistent tangent stiffness components for the discontinuity obtained as a derivatives of the exponential softening laws from (44) with respect to the corresponding displacement jumps. It is worth noting that local computation of discontinuity parameters provides the possibility to perform static condensation at the element level keeping the same number of global unknowns like in standard finite element procedures. Global solution of Eq. (51) can be controlled in incremental iterative way either with arc-length or displacement control. When utilizing the displacement control, the iterative process can be performed by Newton-Raphson iterations with tangential stiffness, or with secant stiffness.

4.7 A Beam Validation Test

In order to verify the mesh independence of the softening response, the beam of length $l = 1$ cm and $b = 1$ cm, $h = 0.8$ cm (cross-section width and height) is subjected to imposed displacements which produce the tension and shear failure. Material parameters of the beam are $E = 1000$ kN/cm^2, $\nu = 0.2$, $N_u = 0.176$ kN, $T_y = 0.015$ kN, $T_u = 0.0176$ kN. Hardening modulus for shear is $\overline{K}_v = 100$ kN/cm^2. Fracture energies for mode I and mode II are $G_f^{(u)} = 15$ N/m, $G_f^{(v)} = 2$ N/m.

Author's personal copy

The beam is discretized with 3, 5 and 10 finite elements, while the initial weakness is introduced into one of them. Fig. 24 shows the beam force-displacement responses. The softening response in both cases, where failure in mode I and mode II happens, remains mesh-independent. This is a consequence of the embedded strong discontinuity formulation where the localized zone is not defined by the size of the element, but by the discontinuity which is represented by the Dirac delta function inside the element.

4.8 Uniaxial Tension Test in the Lattice

Uniaxial tension tests on 2D Timoshenko beam lattice with embedded strong discontinuities for mode I and mode II were performed in [8]. The material is represented as a two-phase heterogeneous composite with stronger (phase I) and weaker phase (phase II). The heterogeneous specimens with initially 40, 50, and 60% of phase II material are subjected to the imposed displacement on the upper boundary causing the stretching of the lattice.

The obtained macroscopic curves for all three specimens (Fig. 25) reveal that the specimens are broken at the end of the loading programme. In the tension test, one dominant macro crack propagated through the specimen and led it to failure.

The influence of heterogeneity on a global response can be studied with such lattice models. Different levels of heterogeneity lead to different failure mechanisms, and even linear elastic response is not the same. With an increase of the amount of weaker phase, the global modulus of elasticity decreases.

The failure patterns of three different heterogeneous specimens are shown in Fig. 26 presenting the final cracks at the end of tension test computations. Namely, one macro crack is present in all of the specimens, and it dominates

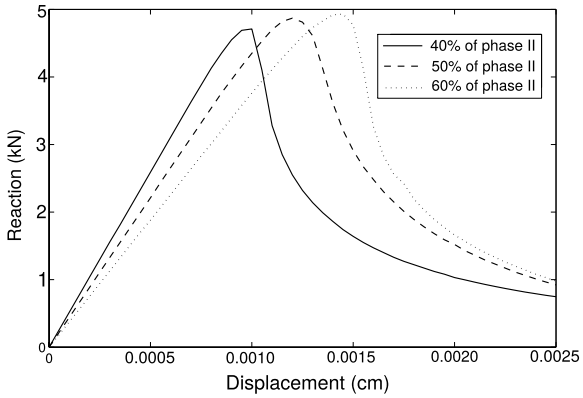

Fig. 25 The computed macroscopic response with different levels of heterogeneity for uniaxial tension test. Taken from [8]

the final failure mechanism. However, in each specimen, the macro crack formed differently depending on the initial heterogeneity, which decides the crack path.

4.9 3D Lattice Model with Enhanced Timoshenko Beam as Lattice Element

The extension of the 2D lattice model presented in the previous subsection is extended towards a 3D space in [9]. This model provides a capability of representing cracks propagating through rock until complete localized failure. The model is based upon the discrete lattice of 3D Timoshenko beams that can capture failure modes by using the embedded strong discontinuities. Failure modes are presented with: mode I or tensile opening, mode II or in-plane shear sliding and mode III or out-of-plane shear sliding, as well as the mixed-mode fracture propagation which is often the dominant mechanism in rock failure. The model can also consider variability of model parameters.

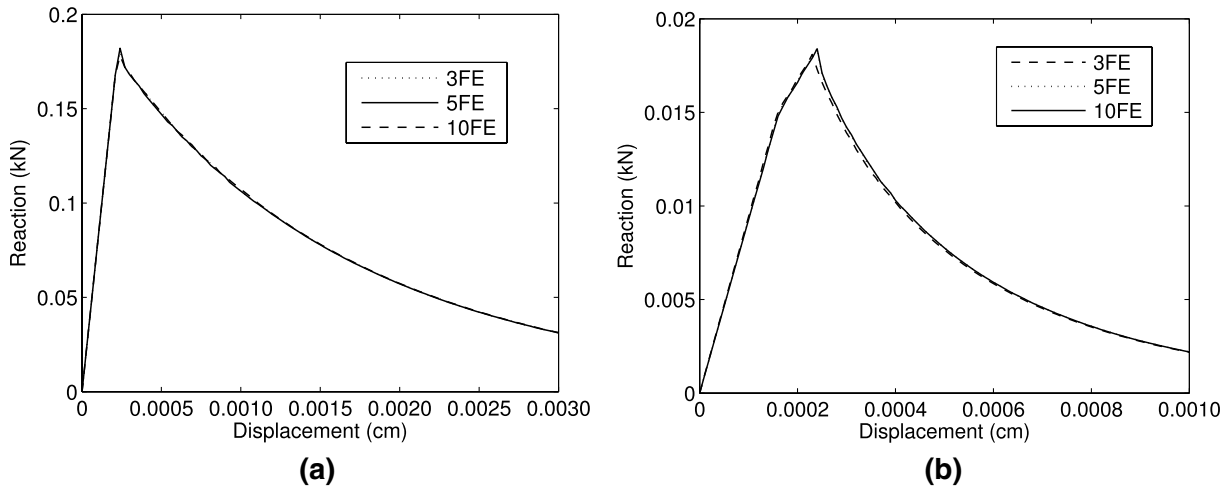

Fig. 24 The computed beam response for: **a** mode I failure and **b** mode II failure. Taken from [8]

Author's personal copy

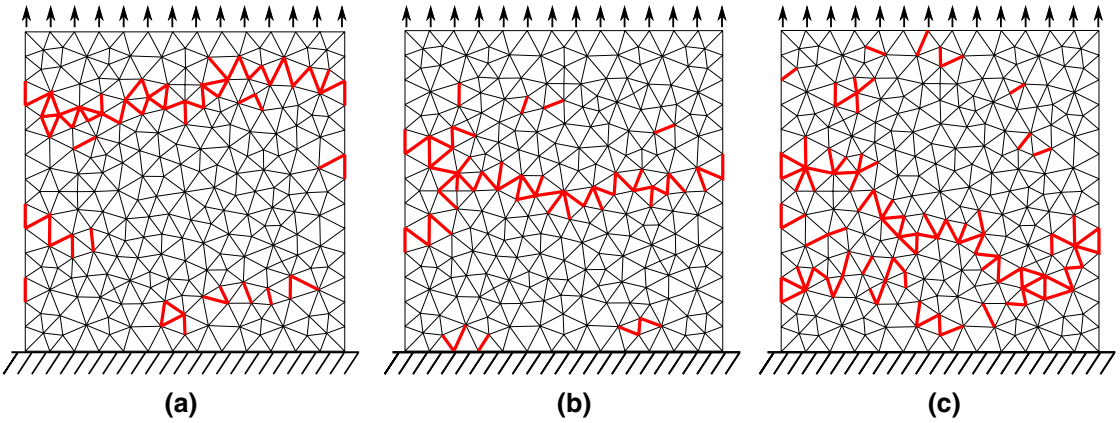

Fig. 26 Final failure patterns created in tension test for specimens with **a** 40% of phase II, **b** 50% of phase II and **c** 60% of phase II (broken links are *red coloured*). Taken from [8]. (Color figure online)

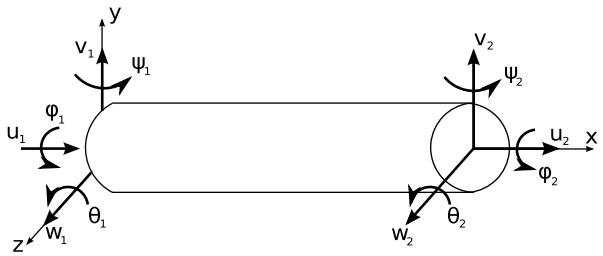

Fig. 27 A 3D 2-node Timoshenko beam

The standard kinematics for a 3D Timoshenko element are

$$\begin{aligned}
\epsilon(x) &= \frac{du(x)}{dx}, \\
\gamma_y(x) &= \frac{dv(x)}{dx} - \theta(x), \\
\gamma_z(x) &= \frac{dw(x)}{dx} + \psi(x), \\
\kappa_x(x) &= \frac{d\varphi(x)}{dx}, \\
\kappa_y(x) &= \frac{d\psi(x)}{dx}, \\
\kappa_z(x) &= \frac{d\theta(x)}{dx}
\end{aligned} \tag{57}$$

where $\bar{\boldsymbol{\epsilon}} = \left[\epsilon \ \gamma_y \ \gamma_z \ \kappa_x \ \kappa_y \ \kappa_z\right]^T$ represents the regular part of the beam strain vector while the displacement vector $\bar{\mathbf{u}} = \left[u \ v \ w \ \varphi \ \psi \ \theta\right]^T$ is given according to displacements shown in Fig. 27. The chosen Timoshenko beam element has 2-node interpolation and a single Gauss point integration, which makes all deformation values constant. In order to construct embedded strong discontinuities one needs to enhance the displacement fields as

$$\begin{aligned}
u(x) &= \sum_{a=1}^{2} N_a(x) u_a + M(x)\alpha_u \\
v(x) &= \sum_{a=1}^{2} N_a(x) v_a + M(x)\alpha_v \\
w(x) &= \sum_{a=1}^{2} N_a(x) w_a + M(x)\alpha_w \\
\varphi(x) &= \sum_{a=1}^{2} N_a(x)\varphi_a, \quad \psi(x) = \sum_{a=1}^{2} N_a(x)\psi_a \\
\theta(x) &= \sum_{a=1}^{2} N_a(x)\theta_a
\end{aligned} \tag{58}$$

Fig. 28 Failure mechanism for two samples obtained within the experiment: **a** the detachment of the material is noticed at the lower part of the specimen, **b** the diagonal failure is pronounced. Taken from [9]

Author's personal copy

Such enhancements lead to construction of mode I, II and III in a similar way like presented for 2D case.

The 3D lattice model was used to simulate the experimental result of the specimen subjected to uniaxial compression test with no lateral confinement (Fig. 28). The experiment showed that the post-peak behaviour of limestone, which is very brittle, is also obtained with the numerical model. Very close macroscopic curves are obtained for three different choices of the finite element mesh (coarse, fine and the finest) (Fig. 29). However, a slight difference in macroscopic curves can be noticed, which is a result of material heterogeneities that were initially distributed according to the Gauss distribution.

In this example, the lower part of the specimen is largely affected by damage and cracking. Moreover, the cracks are irregular throughout the specimen, which is a result of initial heterogeneity. The failure mechanism obtained with the numerical model also corresponds to the experiment. Fig. 29c shows the distinction between the failed elements in mode I, and failed elements in shear modes II and III. Failure in unconfined compression test is strongly influenced by the shear failure. A large number of elements also broke due to mixed mode failure and these overlap on the two figures in Fig. 29c.

4.10 Influence of Specimen Shape Deviations

The 3D lattice model from [9] was used to confirm the experimental findings of unavoidable, but insufficiently investigated influences of the test specimen shape

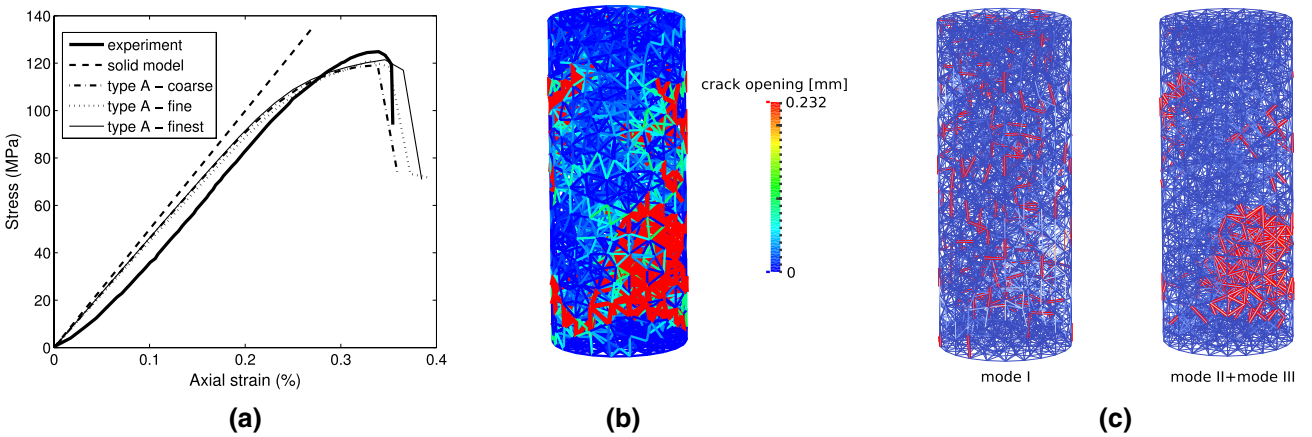

Fig. 29 Unconfined compression test: **a** computed macroscopic response compared to solid model and experiment, **b** crack opening (presented as euclidean norm of all three failure modes) at the end of numerical test for **c** *red* marked elements are broken elements due to: mode I, modes II and III. Taken from [9]

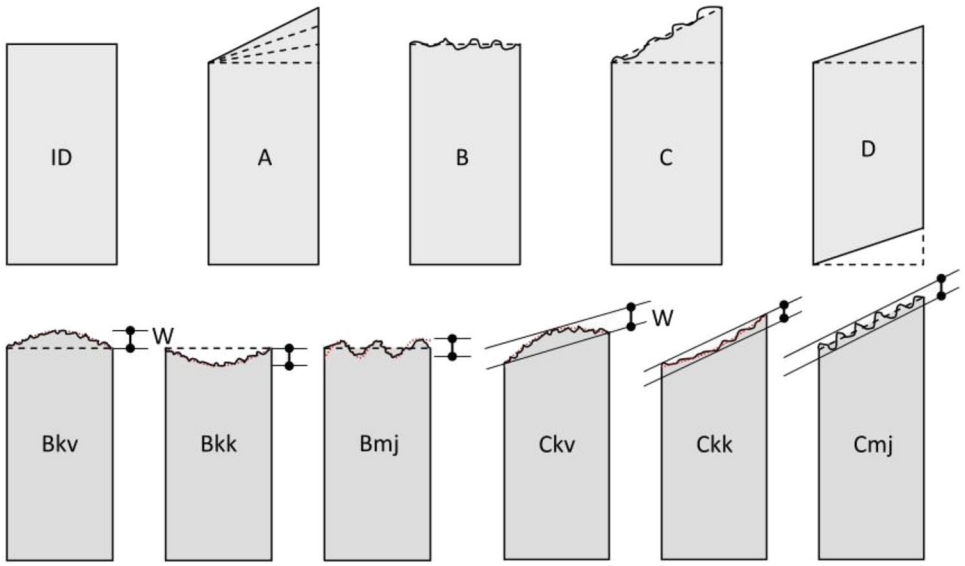

Fig. 30 Basic groups of specimens—ID, A, B, C and D; convex (Bkv, Ckv), concave (Bkk, Ckk) and mixed (Bmj, Cmj) types of non-flatness/waviness for groups B and C. Taken from [79]. (Color figure online)

Author's personal copy

deviations on unconfined compressive strength appearing in testing which can significantly affect the results [79]. It is well known from laboratories that the inaccuracies of the cylindrical specimens resulting with deviations from flatness, perpendicularity and parallelism lead to the reduction of strength and various moduli. The basic groups of specimen shape deviations can be categorized as shown in Fig. 30.

In the presented research [79], ninety intact rock cylindrical test specimens intentionally constructed with initial shape deviations are included. Some of them are also constructed and tested with the numerical model to provide more insight into experimental results and additionally verify the hypothesis. Fig. 31 shows the specimens of the characteristic groups constructed with the numerical model. The reliable representation of the changing boundary conditions in the numerical model due to deviation is achieved by using the penalty contact elements which can properly capture the gradual contact with the load platens, as the consequence of geometrical irregularities of a particular specimen.

The results showed that within the group A, which examines the effect of non-parallelism, no significant changes and drops in the strength were observed compared to the group ID, which represents the 'ideal' specimen. Moreover, similar failure patterns were noticed in these two groups. The group D, with the effect of non-perpendicularity, had similar strengths as the groups ID and A. The effect of non-flatness was investigated through group B, which showed significant drops in strength due to the occurrence of local failure near the irregularities of the base.

5 Lattice Element Models for Transport Processes

Mechanical failure aspects of the materials with lattice element models have been elaborated so far. Simplicity of the lattice models allow us to consider important aspects of quasi-brittle failure such as fine scale effects of the material heterogeneities influencing the failure, localization and complex multiple cracking. However, various transport processes through the material can additionally influence its durability. For example, cracks can occur due to moisture or heat transport inducing internal stresses, or corrosion expansion can damage the reinforcement in the material. Moreover, any quasi brittle material in a close interaction with the fluid will be subjected to additional time dependent degradation and mass transport effect on its durability needs to be examined.

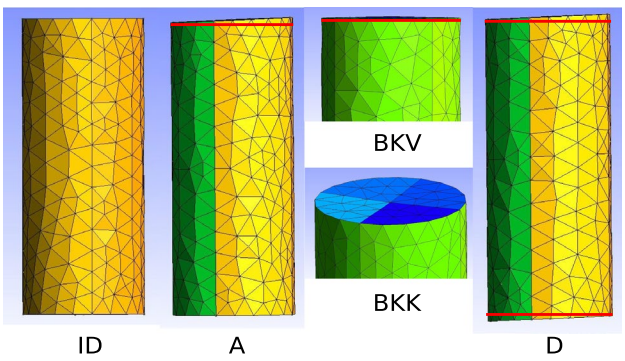

Fig. 31 Representative numerical rock specimens from the observed groups with initial shape deviation. Taken from [79]

Due to advantageous lattice model properties in successful representation of failure, some researchers recently extended the existing lattice models by coupling their mechanical aspects with the mass transport within the lattice. Bolander and Berton [80] developed the model for the shrinkage of concrete due to transfer of moisture by coupling the mechanical lattice model with the diffusion process along one-dimensional conduit lattice elements. Nakamura et al. [81] studied the time dependent drying shrinkage of concrete due to transfer of moisture and degradation of the reinforcement in reinforced concrete due to chloride ions penetration by solving the diffusion equation within the lattice. Diffusivity of the chlorides in cracked concrete with lattice approach was further studied in [82–84]. Grassl [16] developed a lattice element model for flow in cracked concrete by using dual lattices, where one serves for mechanical simulation and the other for flow simulation. This work was extended to simulate the hydraulic fracture with lattice element approach by using the Biot's theory of poro-elastic medium [17]. Nikolic et al. [14, 15] developed the lattice approach to simulate the failure of fluid saturated fractured poroplastic medium based on Biot's theory. Asahina et al. [85] examined the fracture hydro-mechanical aspects of wetting and drying by coupling the lattice model for mechanical behaviour and finite volume model for flow. Hydraulic fracturing application is performed by coupling the lattice element model and discrete element model for rocks in [86].

In this Section, the main aspects of the coupled hydro mechanical lattice approach for the analysis of fluid saturated poroplastic medium with fractures, developed in [14, 15] will be briefly presented. Hydro mechanical lattice model, which can account for transient fluid flow, is based on a mechanical 2D model with Timoshenko beams as lattice elements presented in [8] and in Sect. 4. Localized failure of porous medium is simulated with embedded strong discontinuities positioned inside cohesive links, as presented above. The goal of the coupled model is to simulate the time dependent failure of a fully saturated heterogeneous poroplastic medium. In order to couple the mechanical response of the lattice and the transport of the fluid, Terzaghi and Biot's porous media theory [87, 88] is

Author's personal copy

used, while the recent contributions in porous media can be found in [89]. Fluid flow is governed by diffusion equation and Darcy's law across the lattice network, while special care is taken in computing the lattice permeability (flow) parameters.

5.1 Coupling of the Mechanical Part and Fluid Transport

The equations of the porous medium saturated with a fluid are presented here. Convective terms and gravity acceleration are neglected in this problem. The standard equilibrium equation of a porous medium is given by relation

$$\nabla \cdot \sigma = 0, \tag{59}$$

where the total stress can be decomposed into

$$\sigma = \sigma_s + \sigma_f = \sigma' - bp \tag{60}$$

where subscripts s and f denote the solid and the fluid contribution to the total stress. The effective stress σ' represents the mechanical stress and measures the material properties of the solid skeleton under drained conditions, p is fluid pressure and b is the Biot coefficient. The continuity equation for the fluid flow can be written as

$$\frac{\partial \zeta}{\partial t} + \nabla \cdot v_f = 0 \tag{61}$$

where ζ is the amount of fluid content which is defined as the variation of fluid volume per unit volume of porous material and v_f is the fluid flux. The fluid content can be written as

$$\zeta = \frac{1}{M} p + b \nabla \cdot u_s \tag{62}$$

where u_s represents the displacements of the solid skeleton and M Biot's modulus defined as

$$\frac{1}{M} = \frac{n_f}{K_f} + \frac{b - n_f}{K_s}. \tag{63}$$

where n_f denotes porosity, K_f is the bulk modulus of the fluid, K_s is bulk modulus of the solid and b is the Biot coefficient defined by

$$b = 1 - \frac{K_t}{K_s}. \tag{64}$$

The K_t is the overall bulk modulus of the porous medium. The inclusion of the fluid content (62) into the fluid continuity Eq. (61) results with coupled time dependent diffusion equation

$$\frac{1}{M} \frac{\partial p}{\partial t} + b \nabla \cdot v_s + \nabla \cdot v_f = 0. \tag{65}$$

Vectors v_s and v_f represent the velocities of the solid and the fluid, respectively. The latter is defined by the Darcy law

$$v_f = -k_f \nabla p \tag{66}$$

where k_f is the permeability of the porous medium. The boundary conditions are applied on both the solid and the fluid part of the coupled medium.

One can notice that such formulation brings two coupling mechanisms in fluid structure interaction problem of this kind. Namely, the changes in the pore pressures influence the stress by Eq. (60), while deformation of the mechanical skeleton produces the changes in the flow field by Eq. (65).

5.2 Coupling of the Mechanical and Transport Lattices

The transport of the fluid flow from Eq. (65) is governed across the transport lattice which coincide with the mechanical lattice (Fig. 32). More precisely, the fluid flow is spread across the lattice, where fluid pressure is added as an additional degree of freedom of the lattice element (Fig. 33). While the mechanical part of the lattice uses the beam elements, the transport lattice can be viewed as an assembly of one-dimensional conduit elements (Fig. 34). The cross section of each lattice conduit element is considered as the cross section area available for fluid flow. It is computed as the shortest distance between centroids h_f of the two neighbouring triangles multiplied by the thickness (Fig. 34). Alternatively, dual

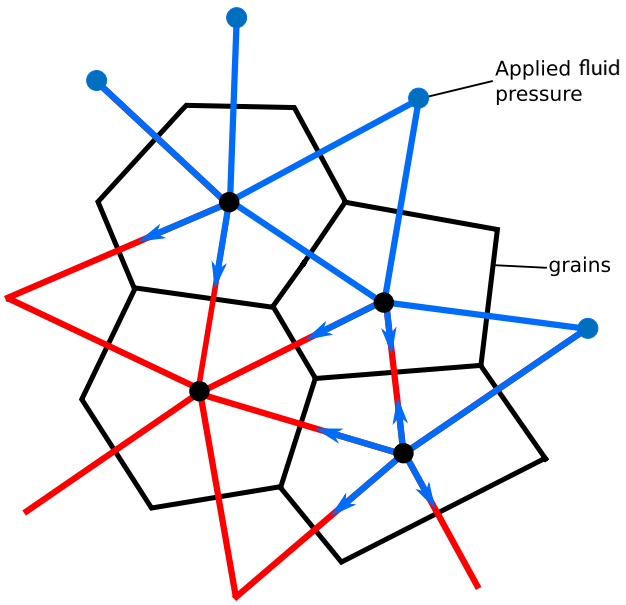

Fig. 32 Transport lattice for the fluid flow. (Color figure online)

Author's personal copy

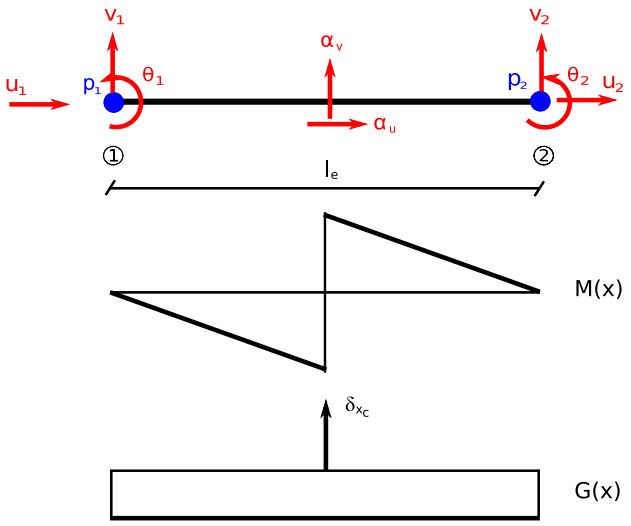

Fig. 33 The enhanced lattice element of Timoshenko beam with its mechanical degrees of freedom and fluid pressure degrees of freedom, discontinuous shape function $M(x)$ and its derivative $G(x)$. (Color figure online)

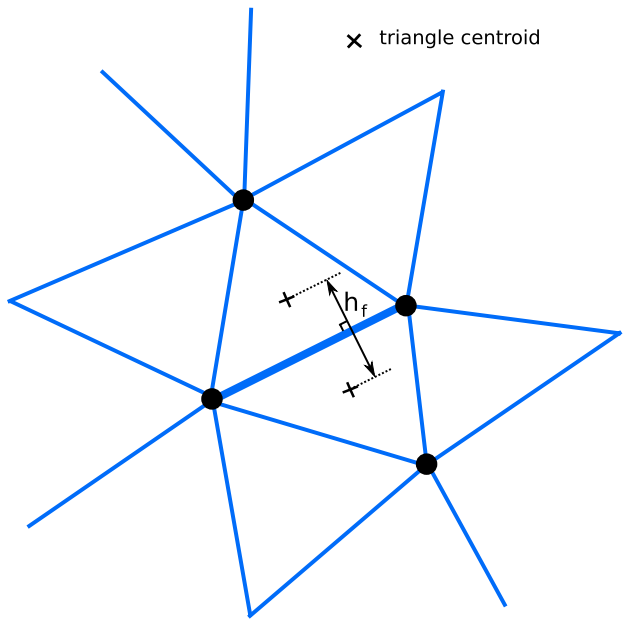

Fig. 34 The fluid flow disposable cross section area

lattice approach, where one lattice is used for mechanical simulation and the other for transport process, is used in [16, 17].

The total stress from Eq. (60) is presented in terms of stress resultants $\boldsymbol{\sigma} = [N \;\; T \;\; M]^T$ and can be decomposed into effective stress resultants and pore pressure forces

$$\begin{bmatrix} N \\ T \\ M \end{bmatrix} = \begin{bmatrix} N' \\ T' \\ M' \end{bmatrix} - b \begin{bmatrix} pA \\ 0 \\ 0 \end{bmatrix} \tag{67}$$

where the effective stress resultant components can be obtained through the Timoshenko beam's elasticities denoted with $\mathbf{D}_{sk}$.

$$\begin{bmatrix} N' \\ T' \\ M' \end{bmatrix} = \underbrace{\begin{bmatrix} EA & 0 & 0 \\ 0 & GA & 0 \\ 0 & 0 & EI \end{bmatrix}}_{\mathbf{D}sk} \begin{bmatrix} \epsilon \\ \gamma \\ \kappa \end{bmatrix} \tag{68}$$

The strain vector is obtained with Eq. (29) from above. The Darcy law from Eq. (66) can be written for the lattice transport model as

$$v_f = -k_f \frac{dp}{dx} \tag{69}$$

One can use the linear shape functions for pressure interpolation $\{N_1^p(x) = 1 - \frac{x}{l_e}, \; N_2^p(x) = \frac{x}{l_e}\}$ and corresponding derivatives $\{B_1^p(x) = -\frac{1}{l_e}, B_2^p(x) = \frac{1}{l_e}\}$ to construct the finite element problem. The pressure interpolation can be written as

$$p(x,t) = \sum_{a=1}^{2} N_a^p(x) p_a(t). \tag{70}$$

while the discretization of the pressure gradient from Eq. (69) results with

$$\frac{\partial p}{\partial x}(x,t) = \sum_{a=1}^{2} B_a^p(x) p_a(t), \tag{71}$$

and the pressure time derivative from Eq. (65) is given as

$$\frac{\partial p}{\partial t}(x,t) = \sum_{a=1}^{2} N_a^p(x) \dot{p}_a(t). \tag{72}$$

The superscript p denotes the pressure interpolation, while the superscript d stands for mechanical displacement and strain interpolation. The generalized nodal pressure field can be denoted with $\mathbf{p} = (p_1, p_2)^T$

The weak form for a coupled problem leads to the finite element residual equation for the mechanical part of the lattice denoted with subscript d

$$\mathbf{r}_d = \mathbf{F}^{ext} - \mathbf{A}_{e=1}^{n_{el}} \int_0^{l_e} \mathbf{B}^{d,T} \boldsymbol{\sigma} dx \tag{73}$$

where the total stress resultants $\boldsymbol{\sigma}$ are obtained in terms of effective stress resultants $\boldsymbol{\sigma}'$ and pore pressures $\mathbf{p}$ in Eq. (67). The symbol $\mathbf{A}_{e=1}^{n_{el}}$ denotes the finite element assembly operator for all element contributions. The effective stress resultants $\boldsymbol{\sigma}'$ are calculated in terms of

Author's personal copy

regular parts of the enhanced strain field. The enhanced strain parameters $\boldsymbol{\alpha}$, due to the embedded strong discontinuity formulation, in each element where localization occurs are obtained by solving the local equilibrium of the effective stresses:

$$\mathbf{h}^{(e)} = \int_{l_e} \overline{\mathbf{G}}\boldsymbol{\sigma}' dx + \mathbf{t}' \tag{74}$$

where $\mathbf{t}'$ represents the corresponding effective stresses acting at the discontinuity. Subsequent static condensation of these parameters allows to keep the standard matrix at the global level.

The coupled fluid Eq. (65) results with the finite element residual form

$$\mathbf{r}_p = \mathbf{Q}^{ext} - \mathbf{A}_{e=1}^{n_{el}} \left[\int_{l_e} \mathbf{N}^{p,T} M^{-1} \mathbf{N}^p dx \dot{\mathbf{p}}_\mathbf{e} - \int_{l_e} \mathbf{N}^{p,T} \alpha \mathbf{B}^d dx \dot{\mathbf{d}}_\mathbf{e} - \int_{l_e} \mathbf{B}^{p,T} k_f \mathbf{B}^p dx \mathbf{p}_e \right] \tag{75}$$

where $\mathbf{Q}^{ext}$ represents the external applied fluxes. Equations (73–75) need to be solved simultaneously to obtain the response for the hydro mechanical lattice approach. The full details of the model can be found in [14].

5.3 Drained Compression Test

The compression test of a fluid saturated rock sample with its boundary conditions (Fig. 35) is presented (see [14] for full details). The external compression load imposed on the top base is applied via constant velocities of $v_0 = 5 \cdot 10^{-4}$ m/s and $v_0 = 1.5 \cdot 10^{-3}$ m/s. Two heterogeneous samples, with a random distribution of stronger and weaker phase, are considered.

Figures 36 and 37 show displacements and pore pressures of heterogeneous samples 1 and 2 plotted in a deformed mesh at the final time step of the simulation. In these two cases, the spatial distribution of the weaker and stronger phase led to different macro crack propagations. It is the strength of the model to consider heterogeneities which influence the failure mechanism together with a fluid flow. Namely, pore pressures remain equal to zero at pervious sides and reach their highest values near the localized zone.

Macroscopic responses (Fig. 38) indicate that higher rates of imposed displacement cause samples to be more resistant with these boundary conditions. This is due to an increase of pore pressure which is brought by a shorter time left for drainage at the sample centre. Such response reveals

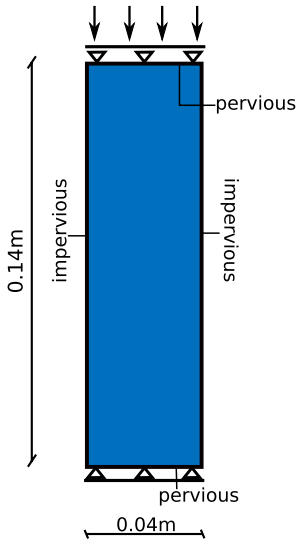

Fig. 35 Geometry of the poroplastic sample and imposed boundary conditions. Taken from [14]

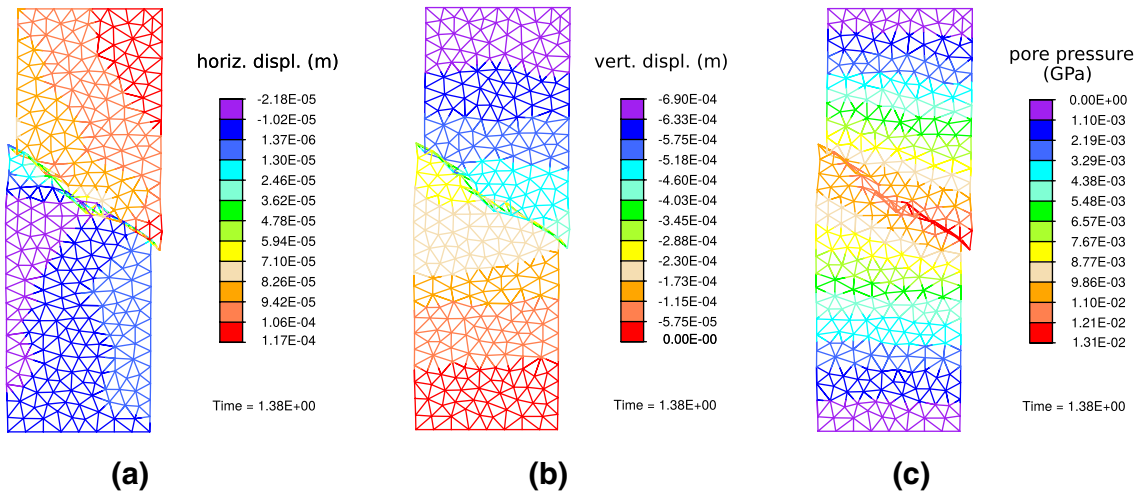

Fig. 36 The state of the 1st heterogeneous sample after the compression test (imposed velocity $v_0 = 5 \cdot 10^{-4}$ m/s): **a** horizontal displacement **b** vertical displacement **c** pore pressure. Taken from [14]. (Color figure online)

Author's personal copy

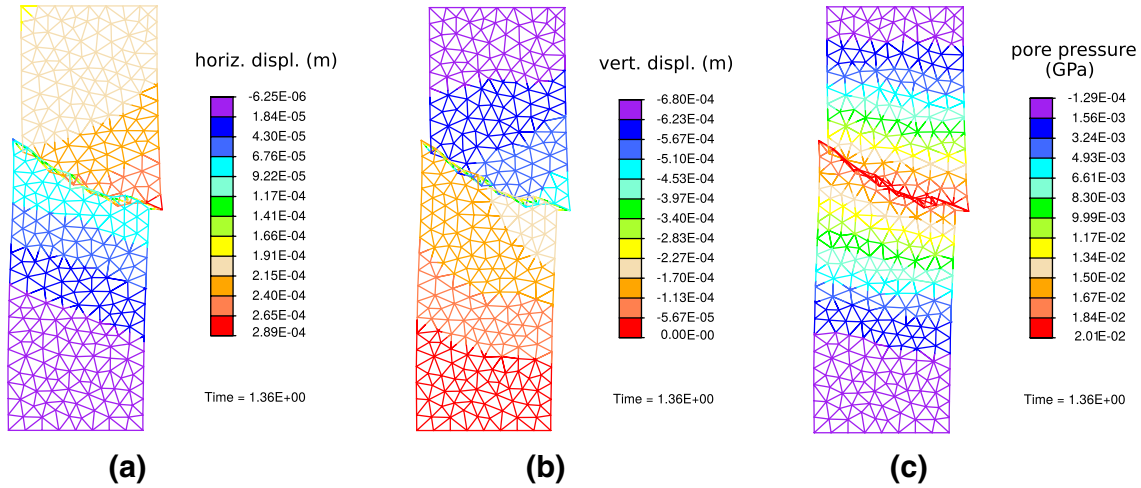

Fig. 37 The state of the 2nd heterogeneous sample after the compression test (imposed velocity $v_0 = 5 \cdot 10^{-4}$ m/s): **a** horizontal displacement **b** vertical displacement **c** pore pressure. Taken from [14]

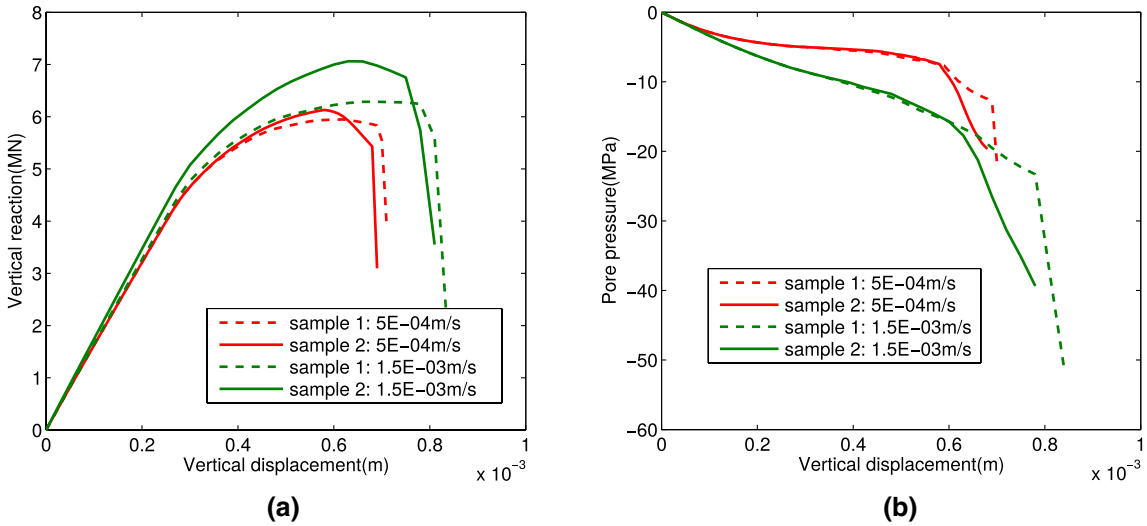

Fig. 38 Macroscopic curves of the poro-plastic sample obtained within the compression test **a** cumulative vertical reaction versus impose displacement **b** pore pressure at the sample centre versus imposed displacement. Taken from [14]

coupling effects which are more pronounced in non linear behaviour and the formation of localization zone.

5.4 Lattice Element Models for Multi-physics Applications

Lattice element models have already been proved to be efficient in coupling the mechanical failure and transport problems. Multi-physics applications of lattice models have been tackled only recently, while there is still a plenty of potential here. Partially saturated porous media formulation could describe the inevitable effects of suctions, which can occur in partially saturated concrete influencing the chloride transport with surface tension in capillaries, or in rocks where strong degradation of the material is present due to wetting and drying. Lattice models could also be used in failure of thermomechanical or piezoelectric materials.

6 Conclusions

Lattice element models are an effective and computationally inexpensive class of discrete models capable of representing important peculiarities of material failure. Among them, the most important ones are capabilities to represent:

Author's personal copy

- linear elastic continuum and uniform straining of the topologically regular or irregular lattice with appropriate computation of lattice element parameters
- localized failure by applying the breaking criterion on the lattice elements, which represents cohesive forces between the particles; the issue of singularity at the crack tip, which is present in linear elastic fracture mechanics, is bypassed by the cohesive crack approach
- complex and multiple crack propagations through the domain where one does not need to worry about the crack interactions
- mesh-independent softening response, with introduction of embedded strong discontinuities by enhancing the kinematics of lattice cohesive link elements to represent displacement jumps.

These favourable properties make the lattice models appropriate to simulate the quasi-brittle failure behaviour at finer scales of the material, like micro-scale or meso-scale. This has been mostly used with quasi-brittle materials such as concrete or rocks. However, lattice models can be used also in dynamic environments and at macro-scale to capture the propagating discontinuities in a structure.

Recent works have shown that transport processes can be coupled with the mechanical response of the lattice model. For example, moisture or heat transport induce internal stresses which can damage the material. The corrosion expansion can damage reinforcement. Any close interaction of the material with a fluid will result with time dependent material degradation reducing its durability. Such multi-physics applications in lattice models are preformed by coupling the mechanical lattice and transport lattice, where the latter can be considered as a lattice of one-dimensional conduit elements. The full, two-way coupling procedure in porous media, is presented in this paper. Thus, one can simulate the key aspects of the material failure mechanisms in a very efficient way, even when including multi-physics interactions.

References

1. Hrennikoff A (1941) Solution of problems of elasticity by the framework method. ASME J Appl Mech 8:A619–A715
2. Schlangen E, Garboczi EJ (1996) New method for simulating fracture using an elastically uniform random geometry lattice. Int J Eng Sci 34:1131–1144
3. Ostoja-Starzewski M (2002) Lattice models in micromechanics. Appl Mech Rev 55(1):35–60
4. Schlangen E, Van Mier JGM (1992) Simple lattice model for numerical simulation of fracture of concrete materials and structures. Mater Struct 25:534–542
5. Schlangen E, Van Mier JGM (1992) Experimental and numerical analysis of micromechanisms of fracture of cement-based composites. Cem Concr Compos 14:105–118
6. Benkemoun N, Hautefeuille M, Colliat JB, Ibrahimbegovic A (2010) Failure of heterogeneous materials: 3D meso-scale FE models with embedded discontinuities. Int J Numer Methods Eng 82:1671–1688
7. Benkemoun N, Ibrahimbegovic A, Colliat JB (2012) Anisotropic constitutive model of plasticity capable of accounting for details of meso-structure of two-phase composite material. Comput Struct 90–91:153–162
8. Nikolic M, Ibrahimbegovic A, Miscevic P (2015) Brittle and ductile failure of rocks: embedded discontinuity approach for representing mode I and mode II failure mechanisms. Int J Numer Methods Eng 102:1507–1526
9. Nikolic M, Ibrahimbegovic A (2015) Rock mechanics model capable of representing initial heterogeneities and full set of 3D failure mechanisms. Comput Methods Appl Mech Eng 290:209–227
10. Vassaux M, Richard B, Ragueneau F, Millard A, Delaplace A (2015) Lattice models applied to cyclic behavior description of quasi-brittle materials: advantages of implicit integration. Int J Numer Anal Meth Geomech 39:775–798
11. Vassaux M, Oliver-Leblond C, Richard B, Ragueneau F (2016) Beam-particle approach to model cracking and energy dissipation in concrete: identification strategy and validation. Cem Concr Compos 70:1–14
12. Cusatis G, Pelessone D, Mencarelli A (2011) Lattice discrete particle model (LDPM) for failure behavior of concrete. I: theory. Cem Concr Compos 33:881–890
13. Cusatis G, Mencarelli A, Pelessone D, Baylot J (2011) Lattice discrete particle model (LDPM) for failure behavior of concrete. I: calibration and validation. Cem Concr Compos 33:891–905
14. Nikolic M, Ibrahimbegovic A, Miscevic P (2016) Discrete element model for the analysis of fluid-saturated fractured poro-plastic medium based on sharp crack representation with embedded strong discontinuities. Comput Methods Appl Mech Eng 298:407–427
15. Nikolic M, Ibrahimbegovic A, Miscevic P (2016) Modelling of internal fluid flow in cracks with embedded strong discontinuities. In: Ibrahimbegovic A (ed) Computational methods for solids and fluids—multiscale analysis, probability aspects and model reduction. Springer, Switzerland, pp 315–341
16. Grassl P (2009) A lattice approach to model flow in cracked concrete. Cem Concr Compos 31:454–460
17. Grassl P, Fahy C, Gallipoli D, Wheeler SJ (2015) On a 2D hydro-mechanical lattice approach for modelling hydraulic fracture. J Mech Phys Solids 75:104–118
18. Kirkwood JG (1939) The skeletal modes of vibration of long chain molecules. J Chem Phys 7:506–509
19. Keating PN (1966) Effect of invariance requirements on the elastic strain energy of crystals with application to the diamond structure. Phys Rev 145:637–645
20. Hassold GN, Srolovitz DJ (1989) Brittle fracture in materials with random defects. Phys Rev 39:9273–9281
21. Cusatis G, Bazant Z, Cedolin L (2006) Confinement-shear lattice CSL model for fracture propagation in concrete. Comput Methods Appl Mech Eng 195:7154–7171
22. Chang CS, Wang TK, Sluys LJ, van Mier JGM (2002) Fracture modeling using a micro-structural mechanics approach I. Theory and formulation. Eng Fract Mech 69:1941–1958
23. Karihaloo BL, Shao PF, Xiao QZ (2003) Lattice modelling of the failure of particle composites. Eng Fract Mech 70:2385–2406
24. Bolander J, Saito S (1998) Fracture analyses using spring networks with random geometry. Eng Fract Mech 61:569–591
25. Green PJ, Sibson R (1978) Computing Dirichlet tessellations in the plane. Comput J 21:168–173

Author's personal copy

26. Bolander J, Sukumar N (2005) Irregular lattice model for quasi-static crack propagation. Phys Rev 71:094106-1–12
27. Berton S, Bolander J (2006) Crack band model of fracture in irregular lattices. Comput Methods Appl Mech Eng 195:7172–7181
28. Grassl P, Jirasek M (2010) Meso-scale approach to modelling the fracture process zone of concrete subjected to uniaxial tension. Int J Solids Struct 47:957–968
29. Grassl P, Gregoire D, Solano LR, Pijaudier-Cabot G (2012) Meso-scale modelling of the size effect on the fracture process zone of concrete. Int J Solids Struct 49:1818–1827
30. Gregoire D, Verdon L, Lefort V, Grassl P, Saliba J, Regoin J-P, Loukili A, Pijaudier-Cabot G (2015) Mesoscale analysis of failure in quasi-brittle materials: comparison between lattice model and acoustic emission data. Int J Numer Anal Meth Geomech 39:1639–1664
31. Griffith A (1921) The phenomena of rupture and flow in solids. Phil Trans R Soc A 221:163–198
32. Irwin G (1957) Analysis of stresses and strains near the end of a crack traversing a plate. J Appl Mech 24:361–364
33. Orowan E (1948) Fracture and strength of solids. Rep Prog Phys 12:185
34. Rice JR (1968) A path independent integral and the approximate analysis of strain concentration by notches and cracks. J Appl Mech 35:379–386
35. Herrmann HJ, Roux S (1990) Modelization of fracture in disordered systems. In: Herrmann HJ, Roux S (eds) Statistical models for the fracture of disordered media. Elsevier, North Holland, pp 159–188
36. Ibrahimbegovic A (2009) Nonlinear solid mechanics: theoretical formulations and finite element solution methods. Springer, London
37. Bazant ZP, Lin FB (1988) Non-local yield limit degradation. Int J Numer Methods Eng 26:1805–1823
38. Bazant ZP, Pijaudier-Cabot G (1988) Non linear continuous damage, localization instability and convergence. J Appl Mech 55:287–293
39. Nguyen VP, Lloberas-Valls O, Stroeven M, Sluys LJ (2011) Homogenization-based multiscale crack modelling: from micro-diffusive damage to macro-cracks. Comput Methods Appl Mech Engrg 200:1220–1236
40. Contrafatto L, Cuomo M, Gazzo S (2016) A concrete homogenisation technique at meso-scale level accounting for damaging behaviour of cement paste and aggregates. Comput Struct 173:1–18
41. Toro S, Sanchez PJ, Blanco PJ, de Souza Neto EA, Huespe AE, Feijoo RA (2016) Multiscale formulation for material failure accounting for cohesive cracks at the macro and micro scales. Int J Plast 76:75–110
42. Oliver J, Caicedo M, Roubin E, Huespe AE, Hernandez JA (2015) Continuum approach to computational multiscale modeling of propagating fracture. Comput Methods Appl Mech Engrg 294:384–427
43. Fish J (2006) Bridging the scales in nano engineering and science. J Nanopart Res 8:577–594
44. Ibrahimbegovic A, Niekamp R, Kassiotis C, Markovic D, Matthies H (2014) Code-coupling strategy for efficient development of computer software in multiscale and multiphysics nonlinear evolution problems in computational mechanics. Adv Eng Softw 72:8–17
45. Rountree CL, Kalia RK, Lidorikis E, Nakano A, Van Brutzel L, Vashishta P (2002) Atomistic aspects of crack propagation in brittle materials: multimillion atom molecular dynamics simulations. Ann Rev Mater Res 32:377–400
46. Bonamy D, Bouchaud E (2011) Failure of heterogeneous materials: a dynamic phase transition? Phys Rep 498:1–44
47. Kalia RK, Nakano A, Vashishta P, Rountree CL, Van Brutzel L, Ogata S (2003) Multiresolution atomistic simulations of dynamic fracture in nanostructured ceramics and glasses. Int J Fract 121:71–79
48. Barenblatt GI (1962) The mathematical theory of equilibrium cracks in brittle fracture. Adv Appl Mech 7:55–129
49. Dugdale DS (1960) Yielding of steel sheets containing slits. J Mech Phys Solids 8:100–104
50. Lilliu G, van Mier JGM (2003) 3D lattice type fracture model for concrete. Eng Fract Mech 70:927941
51. Moes N, Dolbow J, Belytschko T (1999) A finite element method for crack growth without remeshing. Int J Numer Methods Eng 46:131–150
52. Fries TP, Belytschko T (2006) The intrinsic XFEM: a method for arbitrary discontinuities without additional unknowns. Int J Numer Methods Eng 68:1358–1385
53. Fries TP, Belytschko T (2010) The generalized/extended finite element method: an overview of the method and its applications. Int J Numer Methods Eng 84:253–304
54. Jirasek M (2000) Comparative study on finite elements with embedded discontinuities. Comput Methods Appl Mech Engrg 188:307–330
55. Oliver J, Huespe AE, Sanchez PJ (2006) A comparative study on finite elements for capturing strong discontinuities: E-FEM vs X-FEM. Comput Methods Appl Mech Engrg 195:4732–4752
56. Linder C, Armero F (2007) Finite elements with embedded strong discontinuities for the modeling of failure in solids. Int J Numer Meth Eng 72:1391–1433
57. Brancherie D, Ibrahimbegovic A (2009) Novel anisotropic continuum-discrete damage model capable of representing localized failure of massive structures, Part I: theoretical formulation and numerical implementation. Eng Comput 26:100–127
58. Dujc J, Brank B, Ibrahimbegovic A (2013) Stress-hybrid quadrilateral finite element with embedded strong discontinuity for failure analysis of plane stress solids. Int J Numer Meth Eng 94:1075–1098
59. Gedik YH, Nakamura H, Yamamoto Y, Kunieda M (2011) Evaluation of three-dimensional effects in short deep beams using a rigid-body-spring-model. Cem Concr Compos 33:978–991
60. Yamamoto Y, Nakamura H, Kuroda I, Furuya N (2014) Crack propagation analysis of reinforced concrete wall under cyclic loading using RBSM. Eur J Environ Civ Eng 18:780–792
61. Cundall PA, Strack ODL (1979) A discrete numerical model for granular assemblies. Géotechnique 29:47–65
62. Obermayr M, Dressler K, Vrettos C, Eberhard P (2013) A bonded-particle model for cemented sand. Comput Geotech 49:299–313
63. Camborde F, Mariotti C, Donzé FV (2000) Numerical study of rock and concrete behaviour by discrete element modelling. Comput Geotech 27:225–247
64. Ergenzinger C, Seifried R, Eberhard P (2010) A discrete element model to describe failure of strong rock in uniaxial compression. Granul Matter 13:1–24
65. Utili S, Nova R (2008) Dem analysis of bonded granular geomaterials. Int J Numer Anal Methods Geomech 32:1997–2031
66. Obermayr M, Dressler K, Vrettos C, Eberhard P (2011) Prediction of draft forces in cohesionless soil with the discrete element method. J Terramechanics 48:347–358
67. D'Addetta GA, Kun F, Ramm E, Herrmann HJ (2001) From solids to granulates - Discrete element simulations of fracture and fragmentation processes in geomaterials. In: Vermeer PA, Diebels S, Ehlers W, Herrmann HJ, Luding S, Ramm E (eds) Continuous and discontinuous modelling of cohesive frictional materials. Springer, Berlin, pp 231–258

Author's personal copy

68. D'Addetta GA, Kun F, Ramm E (2002) On the application of a discrete model to the fracture process of cohesive granular materials. Granul Matter 4:77–90
69. Ibrahimbegovic A, Delaplace A (2003) Microscale and mesoscale discrete models for dynamic fracture of structures built of brittle material. Comput Struct 81:1255–1265
70. Delaplace A, Ibrahimbegovic A (2006) Performance of time-stepping schemes for discrete models in fracture dynamic analysis. Int J Numer Meth Engng 65:1527–1544
71. Rots JG, Invernizzi S (2004) Regularized sequentially linear saw-tooth softening model. Int J Numer Anal Meth Geomech 28:821–856
72. Simo JC, Oliver J, Armero F (1993) An analysis of strong discontinuities induced by strain-softening in rate-independent inelastic solids. Comput Mech 12:277–296
73. Ortiz M, Leroy Y, Needleman A (1987) A finite element method for localized failure analysis. Comput Methods Appl Mech Eng 61:189–214
74. Simo J, Rifai M (1990) A class of mixed assumed strain methods and the method of incompatible modes. Int J Numer Methods Eng 29:1595–1638
75. Ibrahimbegovic A, Wilson E (1991) A modified method of incompatible modes. Commun Appl Numer Methods 7:187–194
76. Ibrahimbegovic A, Melnyk S (2007) Embedded discontinuity finite element method for modeling of localized failure in heterogeneous materials with structured mesh: an alternative to extended finite element method. Comput Mech 40:149–155
77. Pham BM, Brancherie D, Davenne L, Ibrahimegovic A (2013) Stress resultant models for ultimate load design of reinforced concrete frames and multi-scale parameter estimates. Comput Mech 51:347–360
78. Bui NN, Ngo M, Nikolic M, Brancherie D, Ibrahimbegovic A (2014) Enriched Timoshenko beam finite element for modeling bending and shear failure of reinforced concrete frames. Comput Struct 143:9–18
79. Stambuk Cvitanovic N, Nikolic M, Ibrahimbegovic A (2015) Influence of specimen shape deviations on uniaxial compressive strength of limestone and similar rocks. Int J Rock Mech Min Sci 80:357–372
80. Bolander J, Berton S (2004) Simulation of shrinkage induced cracking in cement composite overlays. Cem Concr Compos 26:861–871
81. Nakamura H, Srisoros W, Yashiro R, Kunieda M (2006) Time-dependent structural analysis considering mass transfer to evaluate deterioration process of RC structures. J Adv Concr Technol 4:147–158
82. Wang L, Soda M, Ueda T (2008) Simulation of chloride diffusivity for cracked concrete based on RBSM and truss network model. J Adv Concr Technol 6:143–155
83. Wang L, Ueda T (2011) Mesoscale modelling of the chloride diffusion in cracks and cracked concrete. J Adv Concr Technol 9:241–249
84. Savija B, Pacheco J, Schlangen E (2013) Lattice modeling of chloride diffusion in sound and cracked concrete. Cem Concr Compos 42:30–40
85. Asahina D, Houseworth JE, Birkholzer JT, Rutqvist J, Bolander J (2014) Hydro-mechanical model for wetting/drying and fracture development in geomaterials. Comput Geosci 65:13–23
86. Damjanac B, Detournay C, Cundall PA (2016) Application of particle and lattice codes to simulation of hydraulic fracturing. Comput Part Mech 3:249–261
87. Biot MA (1965) Mechanics of incremental deformations. Wiley, Chichester
88. Terzaghi K (1943) Theoretical soil mechanics. Wiley, New York
89. Lewis RW, Schrefler BA (1998) The finite element method in the static and dynamic deformation and consolidation of porous media, 2nd edn. Wiley, Chichester